Report of the Expert Panel on the Technical Causes of the Failure of Feijão Dam I

Expert Panel:

Peter K. Robertson, Ph.D. (Chair)

Lucas de Melo, Ph.D.

David J. Williams, Ph.D.

G. Ward Wilson, Ph.D.

December 12, 2019

EXECUTIVE SUMMARY

At approximately 12:28 p.m. local time on January 25, 2019, tailings dam B-I at Vale S.A.'s Córrego do Feijão Iron Ore Mine ("Dam I"), located 9 kilometers (km) north-east of Brumadinho, in the state of Minas Gerais, Brazil, suffered a sudden failure, resulting in a catastrophic mudflow that traveled rapidly downstream.

This dam failure is unique in that there are high quality video images of the event that provide insight into the failure mechanism. The videos clearly show a slope failure within the dam starting from the crest and extending to an area just above the First Raising (the Starter Dam). The dam crest dropped and the area above the toe region bulged outwards before the surface of the dam broke apart. The failure extended across much of the face of the dam and collapse of the slope was complete in less than 10 seconds, with 9.7 million cubic meters (Mm^3) of material (representing approximately 75 percent (%) of the stored tailings) flowing out of the dam in less than 5 minutes (min). The material in the dam showed a sudden and significant loss of strength and rapidly became a heavy liquid that flowed downstream at a high speed. The videos show that the initial failure was relatively shallow and was followed by a series of rapid shallow slips with steep back slopes that progressed backwards into the tailings impoundment. Based on these observations, it is clear that the failure was the result of flow (static) liquefaction within the materials of the dam. The significant and sudden strength loss indicates that the materials within the dam were brittle.

The failure is also unique in that it occurred with no apparent signs of distress prior to failure. High quality video from a drone flown over Dam I only seven days prior to the failure also showed no signs of distress. The dam was extensively monitored using a combination of survey monuments along the crest of the dam, inclinometers to measure internal deformations, ground-based radar to monitor surface deformations of the face of the dam, and piezometers to measure changes in internal water levels, among other instruments. None of these methods detected any significant deformations or changes prior to failure. Post-failure satellite image analyses indicated slow and essentially continuous small downward deformations of less than 36 millimeters per year (mm/year) were occurring on the dam face in the year prior to the failure, with some acceleration of deformation during the wet season. In the lower part of the dam, the deformations measured in the 12 months prior to failure included horizontal deformations ranging from 10 to 30 mm. Such deformations are consistent with slow, long-term settlement of the dam, and would not alone be indicative of a precursor to failure.

The dam's construction history provides insight as to the possible reasons for the failure. The dam was constructed using the upstream construction method over a period of 37 years in 10 raises. No new raisings were constructed after 2013, and tailings disposal ceased in July 2016. The Starter Dam contained features that impeded drainage through the toe. No significant internal drainage was installed during the construction of later raisings, other than small drainage blankets below some of the later raisings, and chimney drains in some of the upper raisings. The drainage blankets and chimney drains in the later raisings were in response to observed seepage from the dam face above the toe during construction. The initial design of the dam established a relatively steep slope. After the Third Raising, a setback was constructed to straighten the alignment of the dam crest. The setback reduced the overall slope of the dam but moved the upper portion of the dam closer to

the pond and also closer to the future internal water level. Pre-failure aerial and satellite images show that, at times during the life of the dam, water was close to the crest of the dam, resulting in weak tailings close to the crest and interbedded layers of fine and coarse tailings within the dam. The setback also moved the upper portion of the dam over weaker, finer-grained tailings.

The lack of significant drainage features, coupled with the presence of less permeable fine tailings layers within the dam itself, resulted in the dam having a high water level. Seepage from the dam face above the toe was observed periodically from as early as the Fourth Raising. Despite tailings deposition ceasing in mid-2016, review of piezometers installed within the dam showed the water level within the dam did not reduce significantly after tailings deposition ended. The water levels in the upper portion of the dam were slowly dropping, but remained high in the toe region. This was predominately due to the high regional wet season rainfall combined with limited internal drainage in the dam. Deep horizontal drains (DHPs, based on their Portuguese language term) were installed in early 2018, and a total of 14 was installed, mostly along the toe of the setback. Following an incident during the installation of DHP 15, further installation of DHPs was not pursued.

Data from pre-failure geotechnical investigations were significant and included drilling, sampling, cone penetration tests (CPTu), field vane shear tests (FVT), and *in situ* shear wave velocity (Vs) profiles. These data provided detailed information regarding the nature, consistency, and distribution of materials, as well as water pressures, within the dam. These data, combined with available aerial and satellite images, allowed the Panel to develop detailed two-dimensional (2D) and three-dimensional (3D) stratigraphic profiles of the materials within the dam.

The Panel carried out new investigations to provide additional information about the materials within and under the dam. One significant finding was that the tailings within the dam had very high iron (ferrous) content (greater than 50%), with very little quartz (less than 10%). The high iron content gave the tailings a high total unit weight of approximately 26 kilonewton per cubic meter (kN/m^3). The historical CPTu data, together with appropriate unit weights and water pressures, indicate that the tailings were predominately loose, saturated, and contractive at large strains. Advanced laboratory testing carried out as part of the Investigation on representative reconstituted samples of the tailings showed brittle strength loss behavior and indicated the presence of bonding. This brittle strength loss also was observed in historical data from FVTs, CPTu, and in some historical laboratory test data. Scanning electron microscope (SEM) images analyzed by the Panel attributed this brittle behavior to bonding, most likely due to iron oxidation. The advanced laboratory testing also showed that loose samples of tailings would accumulate strain under constant load. This accumulation of strain under constant load is referred to as creep. In summary, the tailings were loose, predominately saturated, and bonded. The bonding rendered the tailings stiff and potentially brittle. Combined, these features resulted in a material that had potential for significant and rapid strength loss with ongoing strain. The stiff, brittle character of the tailings is consistent with the lack of observable deformations prior to failure and the sudden, rapid response at failure.

Analyses of the stress state within the dam showed that significant parts of the dam were under very high loading due to the steepness of the dam, the heavy weight of the tailings, and the high internal

water level. The combination of a steep upstream constructed dam, high water level, weak fine tailings within the dam, and the brittle nature of the tailings created the conditions for failure.

The Panel's investigation focused on possible triggers for a sudden and rapid strength loss capable of causing the global failure seen in the video. It was recognized that the triggers could be relatively small, given the high shear stresses and brittle nature of the tailings within the dam prior to failure. It also was recognized that the triggers could be due to the cumulative effect of multiple small events.

No earthquakes were recorded in the region on the day of the failure. Although blasting occurred in the open pit mines in the area, there was no blasting recorded by the closest seismograph to Dam I on January 25, 2019, prior to the failure. Hence, earthquakes and blasting were not triggers of the failure.

Between October 2018 and the date of the failure, a series of nine boreholes was drilled in the central and upper region of the dam. These boreholes were drilled to install inclinometers and piezometers and generally extended through the dam into the natural soil below. The dam showed no signs of distress during this drilling, and no deformations related to drilling were detected. At the time of the failure, people were working on the dam and a drilling rig was being used to install piezometers at the top of the Eighth Raising, in the central upper part of the dam. The depth of this borehole, at the time of the failure, was estimated to be about 80 meters (m) below the dam surface, and the bottom of the borehole was likely in the original ground surface. The localized drilling of the borehole on the day of the failure would not have triggered the observed global failure of the dam, as confirmed by computer simulations.

In general, water levels within the dam were either slowly falling or remaining essentially constant prior to the failure; hence, changing water levels are not considered to be the trigger of the failure. However, heavy rainfall during the annual wet season (from about October 2018 to the time of the failure) likely resulted in a loss of suction, producing a small strength reduction in the unsaturated materials above the water level. A review of rainfall data reveals that the wet season rainfall near the dam prior to the failure was higher and more intense than in the previous several years, although the total rainfall was less than that experienced annually from 2008 to 2011. Computer simulations showed that a small loss of strength (of up to 15 kilopascals (kPa)) in the unsaturated zone above the water level alone would not be sufficient to trigger the observed instability, but could contribute to the failure as discussed further below.

Computer simulations further showed that high shear stresses in the dam resulted in small ongoing internal strains in the dam over time due to creep, which are consistent with the observed small surface deformations observed in satellite imagery from the year prior to failure. The simulations confirmed that such internal creep could be sufficient to trigger strength loss in the tailings and the failure of the dam, a phenomenon known as "creep rupture."

The simulations further showed that internal creep, when combined with the loss of suction discussed above, would be sufficient to trigger the observed global failure of the dam on January 25, 2019.

In summary, the following history created the conditions for instability in Dam I:

- A design that resulted in a steep upstream constructed slope;
- Water management within the tailings impoundment that at times allowed ponded water to get close to the crest of the dam, resulting in the deposition of weak tailings near the crest;
- A setback in the design that pushed the upper portions of the slope over weaker fine tailings;
- A lack of significant internal drainage that resulted in a persistently high water level in the dam, particularly in the toe region;
- High iron content, resulting in heavy tailings with bonding between particles. This bonding created stiff tailings that were potentially very brittle if triggered to become undrained; and
- High and intense regional wet season rainfall that can result in significant loss of suction, producing a small loss of strength in the unsaturated materials above the water level.

The Panel found that the failure and resulting flow slide was the result of flow liquefaction within the tailings in the dam. The history described above created a dam that was composed of mostly loose, saturated, heavy, and brittle tailings that had high shear stresses within the downstream slope, resulting in a marginally stable dam (i.e., close to failure in undrained conditions). Laboratory testing showed that the amount of strain required to trigger strength loss could be very small, especially in the weaker tailings. These were the main components that made flow liquefaction possible.

The Panel concluded that the sudden strength loss and resulting failure of the marginally stable dam were due to a critical combination of ongoing internal strains due to creep, and a strength reduction due to loss of suction in the unsaturated zone caused by the intense rainfall towards the end of 2018. This followed a number of years of increasing rainfall after tailings deposition ceased in July 2016. The calculated pre-failure strains from this combination of triggers match the small deformations of the dam detected in the post-failure analysis of satellite images from the year prior to the failure. The internal strains and strength reduction in the unsaturated zone reached a critical level that resulted in the observed failure on January 25, 2019.

TABLE OF CONTENTS

EXECUTIVE SUMMARY i

TABLE OF CONTENTS v

LIST OF TABLES ix

LIST OF FIGURES vi

1 INTRODUCTION 1
- 1.1 Terms of Reference 1
- 1.2 Organization of the Report 1
- 1.3 Activities of the Expert Panel 2

2 THE FAILURE 3
- 2.1 Description of the Failure 3
- 2.2 Impacts of the Failure 12

3 INVESTIGATION METHODOLOGY 12
- 3.1 Why Did a Flow Slide Occur? 12
- 3.2 What is Flow (Static) Liquefaction? 13
- 3.3 Potential Triggers of the Failure 14
- 3.4 Investigation Steps 15

4 HISTORY OF DAM I 16
- 4.1 Design Approach and Stages of Construction 16
  - 4.1.1 Internal Drainage 18
  - 4.1.2 Stability 19
- 4.2 Geotechnical Investigations 20
- 4.3 Instrumentation of Dam I 20
- 4.4 Activities Post-Tailings Deposition 21
  - 4.4.1 Surface Water Management System 22
  - 4.4.2 Deep Horizontal Drains (DHPs) 22
  - 4.4.3 Seepage 24
  - 4.4.4 Drilling Program Ongoing at Time of the Failure 25

5 DEFORMATION OF DAM I PRIOR TO FAILURE 26

6 MATERIAL CHARACTERIZATION 28
- 6.1 Historical Data 29
  - 6.1.1 Field 29
  - 6.1.2 Laboratory 32
- 6.2 Material Distribution 33
- 6.3 Field Studies by the Panel 34
- 6.4 Laboratory Studies by the Panel 37

6.5 Advanced Laboratory Testing by the Panel 43
6.6 Material Parameters 49

7 WATER MOVEMENT WITHIN DAM I PRIOR TO FAILURE 52
7.1 Introduction 52
7.2 Approach 52
7.3 Rainfall and Infiltration 53
7.4 Two-dimensional Analyses 53
7.5 Three-dimensional Analyses 58
7.6 Observations of the Analyses 58

8 STABILITY AND DEFORMATION ANALYSES – INVESTIGATING VARIOUS TRIGGERS 59
8.1 Approach 59
8.2 Stability of Dam I 59
8.3 Deformation Analysis of Dam I 61
8.3.1 Overall Approach 61
8.3.2 Evaluation of Triggering Mechanisms 61
8.3.3 Stage 2 Deformation Analyses 64
8.3.4 Stage 3 of Deformation Analyses 66

9 CONCLUSIONS 68

10 QUESTIONS 69

ACKNOWLEDGEMENTS 71

LIST OF FIGURES

Figure 1: Locations of Córrego do Feijão Mine Site Looking North in Relation to Belo Horizonte and Brumadinho (Source: Google Earth 3D, Image Dated July 7, 2018) (Text Added by Authors) 3

Figure 2: Overview of Córrego do Feijão Mine Site Looking West (Source: Google Earth 3D, Image Dated July 7, 2018) (Text Added by Authors) 4

Figure 3: Location of Dam I Looking West (Source: Google Earth 3D, Image Dated July 7, 2018) (Text Added by Authors) 4

Figure 4: Dam I Looking North (Source: Google Earth 3D, Image Dated July 7, 2018) 5

Figure 5: Observed Initial Deformation of the Central Part of Crest 6

Figure 6: Bulging Above the Toe of the Dam Approximately One-Third in from the Left Abutment (Right Side of Photograph), Initiated About 0.2 s After the First Observed Deformation at Crest 6

Figure 7: Continued Settlement of the Crest and Bulging Above the Toe with Water Erupting Above the Toe Toward the Right Abutment (Left Side of Photograph) About 5.5 s After the First Observed Deformation at Crest....6

Figure 8: Extensive Settlement of the Crest and Bulging Above Toe with a Second Water Spout in the Region of Bulge About 5.8 s After the First Observed Deformation at Crest....6

Figure 9: Full Development of Slope Failure with Failed Mass Moving out Beyond the Toe at About 6.7 s After the First Observed Deformation at Crest....6

Figure 10: Regression of the Failure 11 s After the First Observed Deformation, as Captured by CAM1....7

Figure 11: Regression of the Failure 18 s After the First Observed Deformation, as Captured by CAM1....7

Figure 12: Final Regression of the Failure 6 min and 25 s After the First Observed Deformation, as Captured by CAM1....8

Figure 13: Just Prior to the First Observed Deformation, as Captured by CAM2....8

Figure 14: Initial Settlement of the Central Part of Crest, as Captured by CAM2....9

Figure 15: Regression of Liquefaction Failure at 60 s After the First Observed Deformation, as Captured by CAM2....9

Figure 16: Regression of Liquefaction Failure at 98 s After the First Observed Deformation at the Crest, as Captured by CAM2....10

Figure 17: Final Regression of Liquefaction Failure 7 min and 44 s After the First Observed Deformation Initiation of Failure, as Captured by CAM2....10

Figure 18: Failure of Dam I: (a) Observed Initiation at the Center of the Crest; (b) 0.2 s After the Observed Initiation, Showing Initial Bulging of the Face; (c) 1.4 s After the Observed Initiation, Showing Escalation; (d) 2.4 s After the Observed Initiation, Showing the Widening Collapse of the Crest and Increased Bulging of the Face; (e) 2.6 s After Observed Initiation; and (f) 3.6 s After Observed Initiation When the Crest and Bulging Join in Failure....11

Figure 19: Dam I Cross-section, Showing Raisings and Stages of Construction....18

Figure 20: Cross-section Showing Deformation Vectors for the Four Quarters Prior to Failure....28

Figure 21: Layout of CPTu Carried Out in 2005, 2016, and 2018....29

Figure 22: Example CPTu Profile for PZE-29-35....30

Figure 23: Example CPTu (PZE-29-35, from Elevation 910 m msl to 878 m msl)....32

Figure 24: Recreated Cross-section 3-3 Based on Historical Data, Expanded to Show Details Under the Dam....34

Figure 25: Aerial View of Failed Dam I, Looking Approximately South-East, Photographed on March 28, 2019 34

Figure 26: Aerial View of Failed Dam I, Looking North, Photographed on March 28, 2019 35

Figure 27: Sample Locations from June 2019 on Post-failure Image 36

Figure 28: Coarse Tailings Sample Locations S6a (Left) and S6b (Right) 36

Figure 29: Google Earth Image Showing Test Locations for the July 2019 Field Program 37

Figure 30: Comparison of Particle Size Distribution Curves from the 2019 Samples with Pre-failure Historical Data 38

Figure 31: SEM Image of Sample 3 Bag 2 – Coarse Tailings 41

Figure 32: SEM Image of Sample 1 Bag 2 – Slimes 41

Figure 33: SEM Image of Coarse Tailings 42

Figure 34: SEM Image of Coarse Tailings (Detail of Box Shown in Figure 33). Region Highlighted with Arrow Shows Bonding Between Particles 42

Figure 35: Gradations Constructed to Represent Average, Coarse, and Fine Gradations for Testing 43

Figure 36: Comparison of CSLs for the Representative Tailings Tested 45

Figure 37: Comparison of Isotropically Consolidated Drained Triaxial Tests on Average Gradation Samples at Different State Parameters that are Dense of CS 45

Figure 38: CID Triaxial Test Result on an Average Gradation Sample Consolidated to 50 kPa Prepared to a State Loose of CS (ψ = +0.09) 46

Figure 39: Results of CAU (K_0 = 0.5) Strain-controlled Triaxial Tests (Coarse and Fine Gradations) 47

Figure 40: Comparison Between an Isotropically Consolidated Strain-controlled Test (CID-TX14) and Anisotropically Consolidated Load-controlled Test (TXDW01) with the Same State (ψ = +0.09) and Coarse Gradation 48

Figure 41: Comparison Between an Anisotropically Consolidated Strain-controlled (CAU-TX25) and Load-controlled Test (CAU-TXDW02) with Same State (ψ = +0.09) and Coarse Gradation 49

Figure 42: Cumulative Distribution of State Parameters for Coarse and Fine Gradations 51

Figure 43: Influence of Internal Zoning on the Phreatic Surface (Modified from Vick, 1990) 52

Figure 44: Location of Selected Piezometers, Water Level Indicators, and CPTus Used for Seepage Calibration 54

Figure 45: Mean Piezometric and Water Levels Relative to Final Measurements on January 25, 2019 55

Figure 46: Calculated Versus Observed Piezometer Values for a 2D Seepage Model on Cross-section 3-3 56

Figure 47: Computed Water Pressures from the 2D seepage model for Cross-section 3-3 57

Figure 48: Pore-water Pressure Profile Beside Top Berm on Cross-section 3-3 58

Figure 49: Schematic Comparison in Behavior Between Soil that has No Strength Loss, Soil with Strength Loss, and Either No Bonding or with Bonding 61

Figure 50: Cross-section 3-3 Showing Calculated Pre-failure Deformations Due to Creep Combined With a 15 kPa Strength Reduction From Loss of Suction from 3D Computer Simulations 67

Figure 51: Cross-section 3-3 Showing Calculated Deformations at Failure Due to Creep Combined With a 15 kPa Strength Reduction From Loss of Suction from 3D Computer Simulations 67

LIST OF TABLES

Table 1: Dam I Construction Details 17

Table 2: XRD Results – June 2019 Samples 39

Table 3: XRD Results – July 2019 40

LIST OF APPENDICES

Appendix A History of Construction

Appendix B Historical Geotechnical Data

Appendix C Historical Instrumentation Data

Appendix D Image Analysis

Appendix E Field Investigation & Laboratory Geotechnical Data and Interpretation

Appendix F 3D Computer Model Development

Appendix G Seepage Analysis

Appendix H Stability And Deformation Analysis

Appendix I Seismic Analysis

Appendix J Glossary of Terms

1 INTRODUCTION

1.1 Terms of Reference

This Report presents the results of the assessment of the technical cause(s) of the failure of Dam I at Vale S.A.'s ("Vale") Córrego do Feijão Iron Ore Mine (the "Investigation") carried out by a panel of four experts in geotechnical engineering with special expertise in water and tailings dams: Peter K. Robertson, Ph. D. (Chair); Lucas de Melo, Ph.D.; David Williams, Ph.D.; and G. Ward Wilson, Ph.D. (the "Panel"). The Investigation was commissioned by Vale.[1] No Panel member previously worked for Vale or on any matter relating to Dam I.

The Panel was instructed to use its expertise and professional judgment to review and assess requested relevant data and technical information to determine the technical cause(s) of the Dam I failure. The Panel did not assess matters relating to potential corporate or personal responsibility for the failure; rather, its mandate was expressly limited to determining the technical cause(s) of the failure.

The Panel relied on assistance from consultants to review historical data and documents, evaluate specific subject areas, conduct field and laboratory testing, and engage in computer modeling. These consultants included: Geosyntec Consultants; Klohn Crippen Berger Ltd. (KCB); Bentley Systems (formerly known as SoilVision); and Geoapp s.r.l. Although the Panel worked with the consultants throughout the Investigation, the conclusions presented in this Report reflect the professional judgment of, and are solely attributable to, the Panel.

1.2 Organization of the Report

The Report is divided into 10 sections and includes 10 Appendices. Section 2 describes the failure, including a commentary of video footage capturing the onset of the failure and a summary of the failure impact. Section 3 explains the Panel's methodology in conducting the Investigation. It details how the Panel identified the mechanism of failure, discusses potential triggers for the failure, and describes the various investigations and analyses carried out by the Panel to determine the trigger(s). Section 4 discusses the history of Dam I, including the design and construction of the dam's 10 raisings over the course of approximately 37 years, the activity recorded by instrumentation and monitoring devices installed at the dam, and certain activities or observations recorded after the final stage of construction. Section 5 presents the analysis of pre-failure deformations undertaken by the Panel, which reviewed the behavior of the dam prior to failure using satellite imaging, radar, and survey data, as well as available video and drone footage. Section 6 details the characterization of the soil and tailings within the dam as well as the natural soils below the dam, using historical field and laboratory data recorded prior to the failure as well as recent field and laboratory studies conducted by the Panel. Section 7 summarizes the analysis of water movement within the dam over time as well as the role of

[1] The panelists and consultants to the Panel were retained by Skadden, Arps, Slate, Meagher & Flom LLP ("Skadden"), legal counsel to Vale. Skadden assisted the Panel, including by facilitating the collection and organization of documents and information relating to the Investigation.

rainfall. Section 8 presents the stability and deformation analyses carried out by the Panel and discusses possible technical causes of the failure. Section 9 summarizes the Panel's conclusions of the ultimate questions presented by the Investigation: what were the technical cause(s) of the failure, and why did Dam I fail when it did? Section 10 provides short-form responses to a series of questions related to the failure.

The Appendices to the Report provide underlying technical detail as well as additional figures and tables. Appendix A presents a full history of construction of the dam, beginning with the pre-dam site setting and continuing through the construction of each raising of the dam, followed by a description of certain activities and observations at the dam after construction finished. Appendix B presents the historical geotechnical field and laboratory data recorded in the years prior to the failure. Appendix C describes the instrumentation and monitoring devices utilized at the dam and presents the data recorded by those devices over the five years prior to the failure. Appendix D presents a detailed image analysis, utilizing satellite, radar, video, drone, and LiDAR data. Appendix E presents the results of the field and laboratory studies conducted by the Panel. Appendix F describes the process of developing the model used to run the stability and deformation analyses. Appendix G details the seepage analysis conducted to understand water movement in the dam. Appendix H details the stability and deformation analyses. Appendix I describes the analyses of seismograph records. A glossary of key terms used is included as Appendix J to the Report.

1.3 Activities of the Expert Panel

The Panel began its Investigation in March 2019 and completed its work in December 2019. The Panel reviewed documents, data, and information obtained from Vale as well as certain third parties,[2] including the following:

- Video footage of Dam I on the day of the failure;
- Documents reflecting the design and construction history of the dam;
- Records relating to activities at the dam;
- Analyses, reports, and presentations regarding the dam;
- Data from instrumentation and monitoring devices installed at the dam;
- Satellite, light detection and ranging laser (LiDAR), and interferometric synthetic aperture radar (InSAR) data;
- Drone footage and photographs of the dam; and

[2] The Panel requested certain information from TÜV SÜD Bureau de Projetos e Consultoria Ltda, an engineering and consulting firm that performed work on Dam I during the relevant time frame, but TÜV SÜD did not provide this information.

- Data from seismic monitoring devices at or near the dam.

Panel members visited Dam I in March and June 2019 to observe its features, the neighboring structures, the local topography, and to obtain representative field samples. The Panel also conducted interviews of various Vale personnel and third parties. In July 2019, the Panel carried out an extensive field-testing program, and the samples obtained during the field testing were examined through detailed laboratory analysis. The Panel also carried out computer modeling, including seepage analyses, and stability and deformation analyses.

2 THE FAILURE

2.1 Description of the Failure

At approximately 12:28 p.m. local time on January 25, 2019, Dam I suffered a catastrophic and sudden failure. The dam released a mudflow that rapidly traveled through the mine's canteen and offices, as well as houses, farms, inns, bridges, and roads downstream. The mudflow traveled downstream reaching the Paraopeba River.

The location of the Córrego do Feijão Mine site, in relation to the city of Belo Horizonte to the north and the town of Brumadinho to the south-west, is shown in Figure 1. Figures 2 through 4 show details of the Córrego do Feijão Mine site and Dam I prior to the failure. The dam was approximately 80 meters (m) high with a crest length of approximately 700 m.

Figure 1: Locations of Córrego do Feijão Mine Site Looking North in Relation to Belo Horizonte and Brumadinho (Source: Google Earth 3D, Image Dated July 7, 2018) (Text Added by Authors)

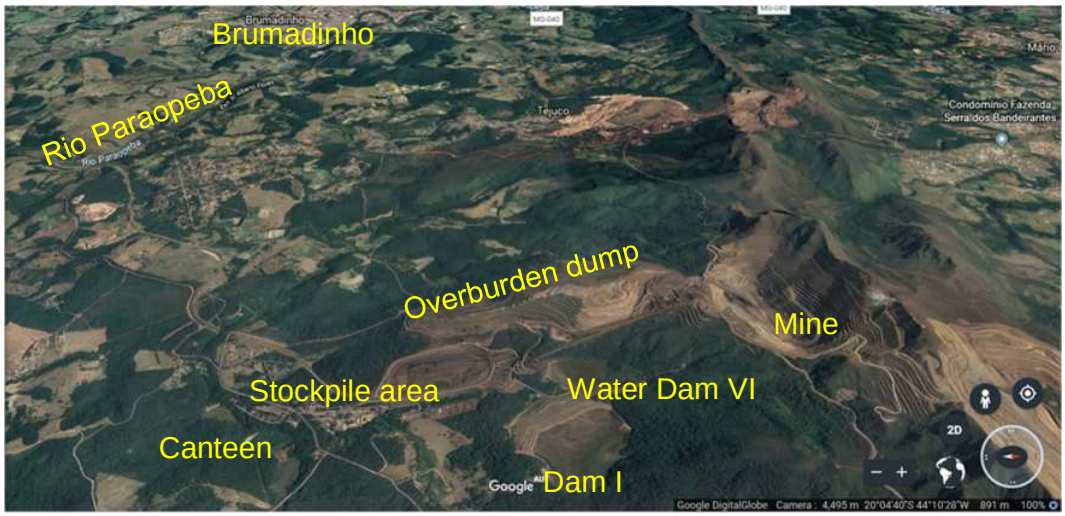

Figure 2: Overview of Córrego do Feijão Mine Site Looking West (Source: Google Earth 3D, Image Dated July 7, 2018) (Text Added by Authors)

Figure 3: Location of Dam I Looking West (Source: Google Earth 3D, Image Dated July 7, 2018) (Text Added by Authors)

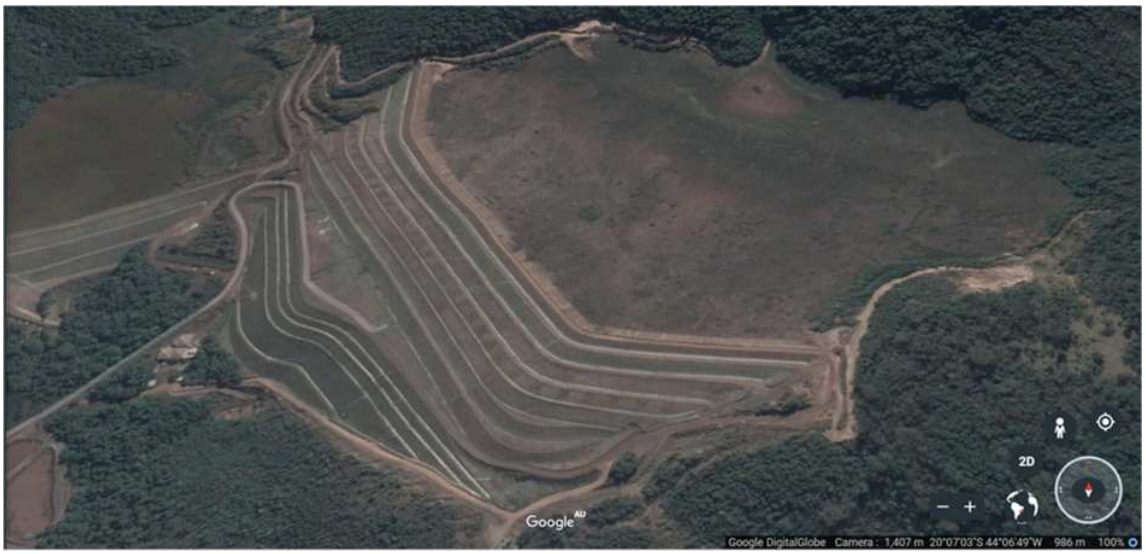

Figure 4: Dam I Looking North (Source: Google Earth 3D, Image Dated July 7, 2018)

The failure initiated and developed very rapidly. The failed material created a mud wave up to a height of about 30 m, which first washed up the downstream face of the adjacent Dam VI. The flow then partially encroached onto the processing plant area opposite Dam I, before engulfing the stockpile area. The flow then swept through the canteen and office complex downstream before coming to a stop in the Paraopeba River on the edge of Brumadinho.

A unique feature of the failure is that video cameras captured the moment it began. Two video cameras were installed in front of and behind the dam. One video camera (CAM1) was located above the processing plant on the opposite side of the valley to Dam I and looked toward the downstream face of Dam I. The other video camera (CAM2) was located at the upstream end of the dam and looked toward the back of the crest of Dam I. A detailed analysis of the video images is provided in Appendix D.

The first observed deformation and early progression of the failure of Dam I are captured in a series of still photographs taken from CAM1, shown in Figures 5 through 11. These images show the progression of the failure, commencing with settlement in the central part of the crest extending over about 80% of the dam (Figure 5). This was closely followed, about 0.2 seconds (s) later, by bulging above the toe of the dam, approximately one-third in from the left abutment (i.e., the right side of the photograph) (Figure 6). The crest settlement and bulging continued to develop rapidly, without any observable deformation of the toe of the dam.

About 5 s after the first observed deformation at the crest, further crest settlement and bulging above the toe occurred and water appears to erupt from the toe region of the dam about one-third in from the right abutment (Figure 7). A second, more turbid, water spout erupted from the toe area, as the surface of the dam in the region of the bulge began to break apart (Figure 8).

Figure 5: Observed Initial Deformation of the Central Part of Crest

Figure 6: Bulging Above the Toe of the Dam Approximately One-Third in from the Left Abutment (Right Side of Photograph), Initiated About 0.2 s After the First Observed Deformation at Crest

Figure 7: Continued Settlement of the Crest and Bulging Above the Toe with Water Erupting Above the Toe Toward the Right Abutment (Left Side of Photograph) About 5.5 s After the First Observed Deformation at Crest

Figure 8: Extensive Settlement of the Crest and Bulging Above Toe with a Second Water Spout in the Region of Bulge About 5.8 s After the First Observed Deformation at Crest

Figure 9: Full Development of Slope Failure with Failed Mass Moving out Beyond the Toe at About 6.7 s After the First Observed Deformation at Crest

CAM1 clearly shows that the failure extends across much of the face of the dam and occurs within the slope of the dam extending from the crest to just above the toe (Figure 9). The slope failure appears to be relatively shallow in depth.

As the failed mass progressed downstream, the failure regressed into the stored tailings as a series of rapid slips, leaving near-vertical back scarps, as shown in Figures 10 through 12. The capture of further progression of the failure by CAM1 became obscured by the dust and mist that rose above the failing mass.

Figure 10: Regression of the Failure 11 s After the First Observed Deformation, as Captured by CAM1

Figure 11: Regression of the Failure 18 s After the First Observed Deformation, as Captured by CAM1

Figure 12: Final Regression of the Failure 6 min and 25 s After the First Observed Deformation, as Captured by CAM1

CAM2 confirmed that the initial failure was relatively shallow and started just behind the crest. CAM2 also clearly shows the regression of the failure into the stored tailings, eventually stopping close to natural ground, as seen in Figures 13 through 17. CAM2 also shows that after each failure slice, the failed material appears to become a heavy liquid.

Figure 13: Just Prior to the First Observed Deformation, as Captured by CAM2

Figure 14: Initial Settlement of the Central Part of Crest, as Captured by CAM2

Figure 15: Regression of Liquefaction Failure at 60 s After the First Observed Deformation, as Captured by CAM2

Figure 16: Regression of Liquefaction Failure at 98 s After the First Observed Deformation at the Crest, as Captured by CAM2

Figure 17: Final Regression of Liquefaction Failure 7 min and 44 s After the First Observed Deformation Initiation of Failure, as Captured by CAM2

A further analysis of the video was conducted in which 4 s of the failure were distilled into 120 frames, as summarized in Figure 18. The dam crest appeared to first deform downward, followed tenths of a second later by initial outward bulging above the toe. This was followed

by initially upward deformation of the area just above the toe that rapidly changed to downward deformation as the crest continued to drop vertically. The slope shows signs of complete failure after about 4 s.

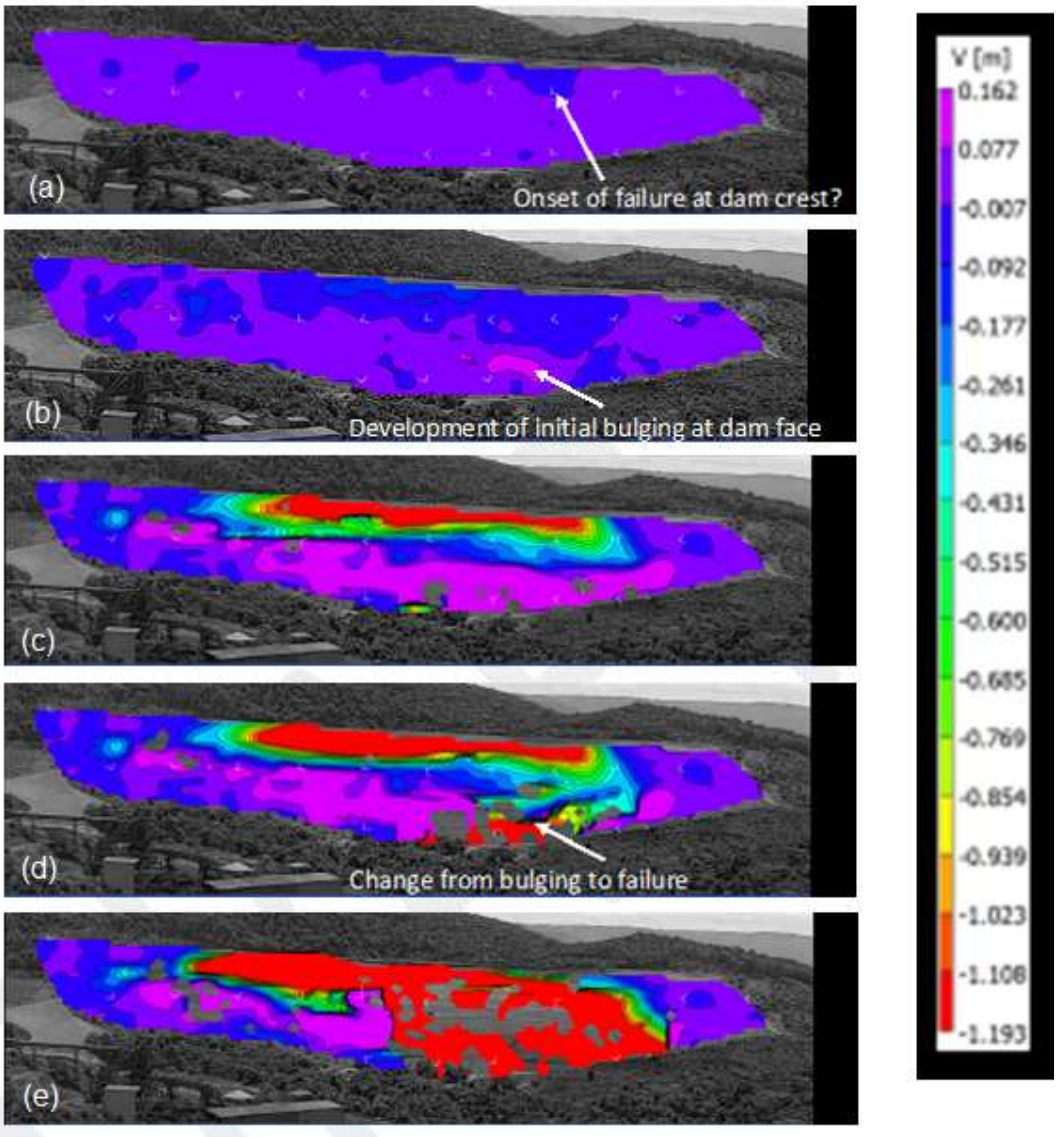

Figure 18: Failure of Dam I: (a) Observed Initiation at the Center of the Crest; (b) 0.2 s After the Observed Initiation, Showing Initial Bulging of the Face; (c) 1.4 s After the Observed Initiation, Showing Escalation; (d) 2.4 s After the Observed Initiation, Showing the Widening Collapse of the Crest and Increased Bulging of the Face; (e) 2.6 s After Observed Initiation; and (f) 3.6 s After Observed Initiation When the Crest and Bulging Join in Failure

The Panel analyzed the seismic records obtained from a nearby seismograph on the day of the failure. The seismic records detected low amplitude ground vibrations starting about 28 s before the first observed deformations of the dam related to the failure. These low amplitude vibrations appear to be the start of internal strength loss occurring in the dam before the full

mechanism of failure was visible on the surface. These vibrations did not have the characteristics of a natural earthquake or a blast. A blast was recorded about 6 min after the failure was observed. Full details are given in Appendix I.

2.2 Impacts of the Failure

As described further in Appendix D, light detection and ranging laser ("LiDAR") was used to determine pre- and post-volumes, and reveals that approximately 9.7 million cubic meters (Mm^3) of material were involved in the failure. This volume represents approximately 75% of the pre-failure volume of about 12.7 Mm^3 of tailings and fill. The maximum tailings thickness was approximately 76 m prior to failure, and the failure eroded up to 3 m of natural ground in the central area of the dam.

More than 250 people perished as a result of the collapse, most of them employees of the mine. The mine's canteen and administrative offices, as well as three locomotives and 132 wagons, were buried in the mine plant area. The mudflow destroyed some parts of the Córrego do Feijão district, including a nearby inn and several rural properties, as well as sections of railway bridge and about 100 m of railway track. Agricultural areas in the valley below the dam were also damaged by the failure.

3 INVESTIGATION METHODOLOGY

The Panel's Investigation addresses the following three questions:

- Why did a flow slide occur?
- What triggered the failure?
- Why did the flow slide occur when it occurred?

This section will explain that the flow slide was the result of a phenomenon called flow liquefaction. It will then explain the Panel's methodology for evaluating the second and third questions regarding the trigger(s) for the failure.

3.1 Why Did a Flow Slide Occur?

As discussed above, videos of the failure provide a clear image of the failure mechanism and reveal that the failure occurred within the slope of the dam as a result of significant and sudden strength loss.

The failure surface appears to be relatively shallow, extending from the dam crest to an area slightly above the toe of the dam, and extends across approximately 80% of the dam area. The dam crest drops almost vertically while the area slightly above the dam toe bulges outward. CAM1 shows that the initial slope failure resulting in the complete breakup of the embankment occurred within a period of about 10 s. After the first slope failure occurs, subsequent thin failure slices occur, extending progressively further into the tailings impoundment. Each failure slice appears to be relatively thin and occurs in rapid succession approximately every 10 s. CAM1 and CAM2 show that the tailings appear to act as a heavy liquid immediately

after failure. CAM2 shows that within a period of about 5 min, the vast majority of the dam tailings had been removed from the impoundment.

Based on the video footage, the failure is the result of flow liquefaction within the materials of the dam. The significant and sudden strength loss indicates that the materials within the dam were brittle.

3.2 What is Flow (Static) Liquefaction?

The phenomenon of soil liquefaction has been recognized for many years. Terzaghi and Peck (1967)[3] referred to "spontaneous liquefaction" to describe the sudden loss of strength of very loose sand-like soils that caused flow slides due to a slight disturbance. Flow liquefaction is also referred to as "static liquefaction."[4] However, because the phenomenon can be triggered by either static or cyclic loading, the term "flow liquefaction" is more commonly used. Flow liquefaction can occur in any saturated or near-saturated meta-stable soil, such as very loose sands and silts as well as sensitive clays. Flow liquefaction has been observed in sensitive clays in Norway and eastern Canada,[5] as well as in tailings dams.[6] For the failure of a soil structure, such as a slope or a dam, a sufficient volume of material must experience strength loss. The resulting failure can be a slide or a flow, depending on the characteristics of the soils and the ground geometry. The deformations resulting from the failure are due to internal, gravity-induced stresses and can occur after the triggering mechanism occurs.

Soil is made up of particles, and shear strength is primarily due to friction between these particles. The magnitude of the shear strength is controlled by the normal (effective) stress between the soil particles, which is controlled by the weight of soil above (i.e., the overburden stress) and the water pressure in the void spaces. The larger the effective overburden stress, the higher the shear strength. When soils are saturated with water, the higher the water pressure, the lower the shear strength. In a slope, the shear stresses driving potential instability are also due to the weight of the ground above. The steeper the slope and the heavier the soils in the slope, the larger the driving shear stresses.

There are void spaces between soil particles. The particles can move under either loading or unloading (shearing), and the void spaces can either decrease (contraction of loose soils) or increase (dilation of dense soils) in volume. The strength loss during flow liquefaction is due to a tendency for the soil to experience rapid volume contraction when sheared. The rapid volume contraction is essentially an internal collapse of the soil structure at the particle level. At some depth, the void spaces of soil are filled with water, and when the tendency for rapid

---

3 Terzaghi, K., & Peck, R. (1967). *Soil mechanics in engineering practice* (2nd ed.). New York: John Wiley.

4 E.g., Jefferies, M., & Been, K. (2015). *Soil liquefaction: A critical state approach* (2nd ed.). Boca Raton, FL: CRC Press.

5 E.g., Geological Survey of Norway. (n.d.). Quick clay and quick clay landslides. Retrieved from https://www.ngu.no/en/topic/quick-clay-and-quick-clay-landslides

6 E.g., Martin, T., & McRoberts, E. (1999). Some considerations in the stability analysis of upstream tailings dams. Proceedings from Tailings and Mine Waste '09: *The 13th International Conference on Tailings and Mine Waste*. Edmonton, AB: University of Alberta Geotechnical Centre.

volume contraction occurs quickly, the stress on the soil is transferred to the water, resulting in a rapid rise in water pressure. This rapid rise in water pressure causes a rapid decrease in the effective normal stress between the soil particles, and the particles can then essentially float in the water. This decrease in effective normal stress between the soil particles can result in rapid and significant loss of shear strength.

Strength loss due to flow liquefaction occurs when either loading or unloading result in sliding between the soil particles, producing a tendency for rapid volume contraction.

To have instability in a dam due to flow liquefaction, the following conditions are required:

- Loose saturated materials that have a tendency for rapid volume contraction under load, resulting in low (liquefied) undrained shear strengths;
- High shear stresses in the slope relative to the liquefied undrained strengths;
- Event(s) that can trigger loss of strength in the materials; and
- A sufficient volume of loose saturated materials for instability to manifest.

3.3 Potential Triggers of the Failure

There are many events that can trigger flow liquefaction. The following is a list of the potential triggers considered by the Panel:

- Rapid loading, such as construction or tailings deposition;
- Rapid cyclic loading, such as earthquakes or blasting;
- Fatigue loading, such as repeated blasting;
- Unloading, such as:
    - Rising water levels within the soil; and
    - Movements, such as within the foundation or due to weak layers;
- Internal erosion and/or piping;
- Human interaction;
- Localized loss of strength due to inflow from underground springs;
- Loss of suction and strength in unsaturated zones above the water level; and
- Internal creep (strains that develop with time under constant load).

3.4 Investigation Steps

To determine which of these events triggered the failure of Dam I and why the failure occurred when it did, the Panel carried out the Investigation in a series of steps which are summarized below:

- Observe the failure through video review;
- Review background documents;
- Interview relevant personnel;
- Observe the dam through field visits;
- Investigate possible deformations prior to the failure, such as:
    - Deformation measurements:
        - Survey monuments
        - Inclinometers
    - Integrated analyses of available images, such as:
        - Video
        - Ground-based radar
        - Laser (LiDAR)
        - Satellite (InSAR and photographs)
        - Drone videos
- Understand the distribution and condition of the materials in and under the dam;
- Understand the materials' behavior;
- Understand the role of water;
- Evaluate potential seismic activity;
- Review human interactions and activity at the dam; and
- Numerically model and test the dam behavior to investigate and eliminate possible trigger events.

4 HISTORY OF DAM I

The history of Dam I, including aspects of the design and construction, are discussed in detail in Appendix A. Appendix A includes a description of the site and surrounding area, as well as the design and construction of each raising of the dam. It also summarizes significant activities and key events that inform an understanding of the structure and characteristics of the dam.

Field investigations and laboratory testing conducted prior to the failure of the dam are presented in Appendix B. Details of the instrumentation and monitoring devices installed at the dam and the associated data are presented in Appendix C.

4.1 Design Approach and Stages of Construction

Dam I was developed to store tailings that were produced during mining operations at the Córrego do Feijão Mine. Dam I was constructed in an area underlain by banded gneisses bedrock, which is overlain by saprolite, residual, and colluvial soils. The dam was located in a valley near the mine, where dam construction could create a substantial disposal capacity for tailings. By constructing the dam, the creek at the base of the valley was blocked, necessitating a process for routing water from the stream to the Feijão Creek downstream of the dam. The construction of the dam and the impoundment of tailings eliminated the creek as a discharge point for groundwater, resulting in an increase in groundwater elevations in the tailings as development proceeded.

Dam I was constructed over a 37-year period from 1976 to 2013 in 15 stages, corresponding to 10 raises. A summary of the history is shown in Table 1, and the raises and stages are illustrated schematically in the cross-section in Figure 19. As shown in Figure 19, the Fourth Raising was set back compared to the previous three raisings, resulting in the straightening and modification of the dam centerline. The setback reduced the overall slope of the dam but moved the upper portion of the dam over weaker, finer tailings and brought water closer to its face. Having water closer to the face also can limit surface drying of the deposited tailings from exposure to sun and wind. No new raisings were constructed after 2013, and the placement of tailings ceased in July 2016.

The dam was constructed using the upstream method with each raise consisting of a berm built on top of previously deposited and dewatered tailings. The materials used to construct the dam raisings in most cases were obtained from the tailings on the beach close to the crest of the dam. When tailings were excavated from the beach close to the dam, the resulting excavations would create weak spots under future raisings due to rapid infilling with whole tailings.

Upstream construction resulted in movement of the crest upstream over time, as illustrated in Figure 19. Using this method, the dam was constructed to a total height of 86 m (toe to crest), with a final crest elevation of 942 meters above mean sea level (m msl) and a crest length of 720 m. The height of each raising varied from 5 m to 18 m. The upstream and downstream slopes of the berms constructed in each raising varied from 1.5 horizontal to 1 vertical (1.5H:1V) to 2.5H:1V; however, slopes of 2H:1V were used in most cases.

Table 1: Dam I Construction Details[7]

Stage	Year	Raising ID	Top Elevation (m msl)	Height max (m)	Project Design Firm	Construction Company
1	1976	Starter Dam (first)	874	18	Christoph Erb	Emtel
2	1982	Second	877	21	Tecnosan	Tercam
3	1983		879	23		Unknown
4	1984		884	28		Construtora Sul Minas
5	1986		889	33		Unknown
6	1990		891.5	35.5		Unienge Com. e Constr. Ltda.
7	1991	Third	895	39	Chammas Engenharia	Construtora Sul Minas
8	1993		899	43		Unknown
9	1995	Fourth	905	49	Tecnosolo	CMS Constr. S.A.
10	1998	Fifth	910	54		U & M
11	2000	Sixth	916.5	60.5		Constr. Dragagem Paraopeba
12	2003	Seventh	922.5	66.5		Construtora Impar Ltda.
13	2004	Eighth	929.5	73.5		Integral
14	2008	Ninth	937.0	81.0	Geoconsultoria	Integral
15	2013	Tenth	942.0	86.0	Geoconsultoria	Salum Enga

[7] Periodic Review of Dam Safety of the Córrego Feijão Mine – Dam I Technical Report (TÜV SÜD 2018) ("2018 TÜV SÜD Periodic Safety Review").

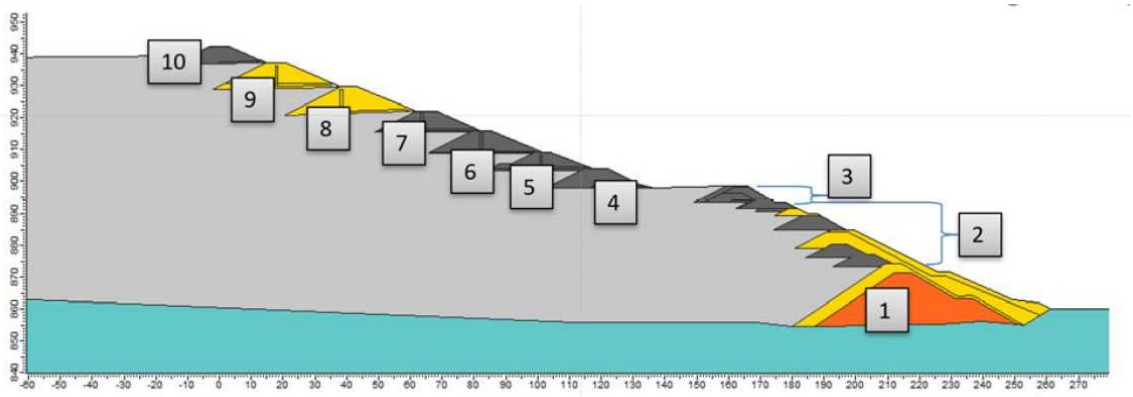

Figure 19: Dam I Cross-section, Showing Raisings and Stages of Construction[8]

The subsections below provide a summary of the main design features and specifications for the dam, based on drawings and text provided in the design documents for each raising. Because as-built drawings were either not prepared or not available for review, many of the design features and specifications described below are based on the Panel's understanding of the plan for dam construction, rather than confirmation of what was constructed.

4.1.1 Internal Drainage

The Starter Dam had no internal drainage features to direct seepage from the impoundment to the face of the dam, which would have reduced the water pressure acting against the dam and increased its stability. The design called for the construction of a layer of laterite soil on the upstream and downstream slopes of the Starter Dam. The Panel could find no record of the design or construction of drainage features to transmit seepage from within or behind the Starter Dam through these laterite layers.

The design of each subsequent raising, except for some stages of the Second Raising, included internal drainage features intended to facilitate dewatering of the adjacent tailings. For the Second, Third, and Fourth Raisings, the design included internal drainage features that typically consisted of a horizontal drainage layer at the base of the berm comprised of either sinterfeed or gravel and a longitudinal collection pipe that drained to a concrete channel on the downstream slope. For the Fifth and subsequent Raisings, the designs specified internal drainage systems consisting of vertical and horizontal drainage layers ("filters") constructed in an "L" shape and small plastic polyvinyl chloride (PVC) pipes designed to direct drainage into perimeter concrete channels at the bottom of the downstream slope of the raising.

The designs for the Second, Third, Fourth, and Fifth Raisings specified a low permeability layer on the upstream slope. The design for the Ninth and Tenth Raisings specified the upstream slope and crest of the berm would be covered in lateritic gravel. For nearly all the

[8] 2018 TÜV SÜD Periodic Safety Review. Numbering added by authors.

raisings, the design documents specified the downstream slopes of the berms should be covered in grass, presumably to prevent surface erosion.

Although toe drains and blanket drains were constructed in most raisings, the overall tailings dam had very little drainage because the upstream berms were built with low permeability materials. This, in addition to the fact that inadequate internal drainage had been installed in the dam during initial construction, contributed to high water levels in the dam and impoundment.

4.1.2 Stability

The design documents indicate stability computations, with associated design factors of safety (FS), were completed for each raising, although the type and complexity of stability calculations varied between the raisings and generally became more sophisticated and detailed as time progressed. The historical stability calculations used shear strength parameters that varied depending on engineering assumptions, and these variations contributed to some of the changes in the calculated FS over time.

Stability calculations were performed for multiple raisings; undrained conditions were considered in stability calculations for the Fifth Raising onwards. Based on analyses for the Starter Dam, Second, and Third Raisings, the designers concluded the design achieved satisfactory FS for drained conditions. In the design documents for the Fourth Raising, the stability calculations yielded FS that were considered by the designers to be below values that they would consider ideal. In addition, during the design and/or construction of the Fourth Raising, seepage was observed on the face of the dam, representing conditions that were considered by the designers to be "very unfavorable" and "not recommended for the safety of the dam."[9]

Stability calculations for the Fifth Raising further identified potentially unstable conditions, including a possibility of dynamic liquefaction leading to an undrained strength condition. The design documents for the Sixth Raising indicated that stability calculations were performed, assuming scenarios in which the materials exhibited drained and undrained strengths. The Sixth Raising design report also recognized the destabilizing effects of high piezometric conditions, and designers indicated that the calculated FS were lower than required. For the Seventh Raising, the FS values resulting from stability calculations for drained and undrained conditions were deemed acceptable by the designers.

Stability calculations were not included in the available design documents for the Eighth Raising. In the design documents for the Ninth and Tenth Raisings, stability analyses were performed for 10 cross-sections. A seepage model was created to estimate the elevation of the water in the dam (i.e., phreatic conditions) that would exist after the berms had been raised and tailings deposited.

[9] See Appendix A.

4.2 Geotechnical Investigations

Geotechnical investigations took place in connection with the design of various raisings. The Panel generally did not rely on the data gathered during the early investigations because the Panel did not consider the data to be adequately documented. Several comprehensive geotechnical investigations were conducted in 2005, 2016, and 2018, the details of which will be discussed in Section 6 and are further detailed in Appendix B.

4.3 Instrumentation of Dam I

The following instrumentation and monitoring devices were installed at or near Dam I:

- Piezometers and water level indicators;
- Inclinometers;
- Flow meters;
- Survey markers;
- Rain gauges;
- Weather stations; and
- A reservoir gauge.

Information on each type of instrument and the data recorded over the five-year period prior to the failure are presented in Appendix C. The survey markers are discussed in Section 5 and are further described in Appendix D.

Piezometers and Water Level Indicators: The piezometers were mostly Casagrande type standpipes with a measurement zone of approximately 1 m in length near the bottom of the standpipe. The piezometers were installed at various depths and mostly clustered in the central region of the dam. Piezometer data were available for 113 piezometers installed from April 1996 up to the failure, although not all data were sufficiently reliable for use by the Panel. Prior to September 2018, almost all piezometers were read manually on an approximate monthly basis. Around August 2018, measurements at approximately half of the piezometers were automated using electrical sensors (pressure transducers) that were placed inside the pre-existing standpipes. Monthly readings were taken on the automated sensors up to December 2018. Starting on January 10, 2019, the automated piezometers were connected to a data-logger and data were recorded at 5-min intervals up until failure.

Shallow water level indicators (INAs, based on their Portuguese language term) also were installed in the downstream face and adjacent to the dam, and were comprised of an open standpipe with a full-length measurement zone. Data were available for 50 water level

indicators, some extending back to 1995, although not all of the data were sufficiently reliable for use by the Panel. Over 40 water level indicators were actively recorded at various intervals.

Inclinometers: Data were reported for six active inclinometers that were installed across Dam I within the embankment and tailings. These inclinometers were read manually. Data for two inclinometers were available from May 2016 to December 2018, with readings taken approximately every other month over that time period. The remaining four inclinometers were installed in early December 2018 and were measured only once in late December 2018, which did not allow relative measurements to be determined. Data from inclinometers indicated no significant relative or absolute deformations.

Flow Meters: Flow meters were used to measure the flow of water coming from subsurface drains at the location where they discharged to surface drainage channels. Information is available for more than 50 drains, which were installed as early as 1990. Data from these flow meters generally show relatively low flows, despite the high water levels present in the dam, which indicate that the drains serve as near-surface features rather than a dam-wide drainage system.

In addition to the relatively shallow drains that were installed during construction, data were available for deep horizontal drains (DHPs, based on their Portuguese language term) installed in 2018. Measurement data for these locations were available for May through July 2018 and October through December 2018, and indicated that flows from the DHPs were between 2.6 and 7.3 m^3/hr (Appendix C).

Rain Gauges and Weather Stations: Rainfall and climate data were available from multiple rain gauges and weather stations located at or nearby the dam, monitored either by Vale or by the Brazilian Federal Government. Rain and weather data were used in the calculation of the water movement within the dam and are discussed in Section 7 as well as in Appendices C and G.

Reservoir Gauge: A reservoir gauge was installed to measure the elevation of the surface water within the tailings pond. Reservoir levels were measured manually between 2006 and 2017. It is understood that after tailings were no longer placed in the impoundment, the level of water in the tailings pond dropped to a level below that which could be measured using the reservoir gauge.

4.4 Activities Post-Tailings Deposition

After the Tenth Raising berm was completed in 2013, no further construction occurred to raise the elevation of Dam I. No tailings were placed after July 2016, but some activities were conducted and observations recorded that provide information related to the condition and performance of Dam I after July 2016. This Section describes the activities and events that occurred after completion of the Tenth Raising, relating to surface-water management activities, installation of DHPs, the occurrence of seepage, and drilling work. Further details are available in Appendix A.

4.4.1 Surface Water Management System

Between July 2016 and the date of the failure, activities associated with the surface water management system involved managing the water level in the impoundment area and maintaining the surface water management features on the face of the dam so that they would transmit water away from the dam.

After Dam I stopped receiving tailings in July 2016, efforts were made to remove water from the tailings impoundment area. The volume of water in the impoundment area was significantly reduced after May 2016 by pumping water to the decant tower, resulting in a shallow depth of standing water in the impoundment far from the dam. In 2018, the diversion of water from a surface spring at the rear of the impoundment to the decant tower was completed. Throughout the remaining operating period, there were various reports of maintenance needs and repairs to the impoundment surface water dewatering system. In the several months before the failure, there were reports of the pumps at the dam not working and being repaired, as well as reports of disconnection and repair of the piping used to route water from the pumps to the spillway tower.

The design of the dam included surface water drainage features to route water from the face of the dam. The surface drainage system consisted of a set of concrete lined channels to route water laterally and down the face of the dam to the creek. Maintenance included periodic removal of sediment that accumulated in the channels and reconstruction of surface channels. In particular, in 2018, several channels were cleared of silt, grading was performed to improve inappropriate drainage in several areas, and vegetation was removed to prevent flow from being restricted. In July 2018, damming of the spring entering the back end of the impoundment was completed with the objective of diverting water from entering the impoundment. Improvements of the damming and diversion systems continued until late 2018, as detailed in Appendices A and D.

Also, as part of the efforts associated with enhancing the management of surface water, two channels were reconstructed between September and December of 2018. One of these channels was located near the dam's left abutment; the other channel was located in the vicinity of DHP 15.

4.4.2 Deep Horizontal Drains (DHPs)

Beginning in late 2017, the installation of DHPs was considered as a possible mechanism to reduce the water levels within the dam to improve stability. The installation procedure for the DHPs included the following main steps:

- Drilling was advanced with air pressure, using a disposable drill bit at a 5% upward angle through the compacted berms;
- Steel casing was then introduced, and the hole was extended using water, with clean water return normally achieved, which was directed to a surface channel downslope; and

- A 50 mm PVC horizontal drain was then installed, and the first 25 m were then grouted with a cement/bentonite mixture.

The size of the compressor was specified to achieve 100 m depth, and installation procedures stated that the compressor "works on demand" up to 600 kPa (i.e., up to 60 m of water head). The tailings in the dam were found to be very soft, requiring little torque to advance the drill bit. Advancing the drilling was mainly achieved by pressure (air and/or water), with minor rotation to relieve rod friction. A constant water pressure of about 400 kPa was then added to the air pressure (nominally 600 kPa), giving a total pressure of up to 1000 kPa, to advance drilling beyond a depth of 40 m.

DHP installation started in March 2018, and by May 2018, 13 DHPs were installed. Eight of the initial DHPs were located along the toe of the setback through the Fourth Raising. Two DHPs were installed through the Eighth Raising and one through the Sixth Raising, but little to no flow was recorded at these three DHPs. Two DHPs were installed near the toe of the dam: one near the right abutment and one near the left abutment. Field logs were available for review and indicated that none of the DHPs reached the length originally intended (i.e., 100 m); the typical length was about 60 m, with a maximum reported length of just over 80 m. Records of flow recorded from the DHPs are provided in Appendix C.

In June 2018, the installation of the remaining DHPs began, and no issues were reported with the installation of DHP 14 through the Fourth Raising at the toe of the setback. However, during the installation on June 11, 2018 of DHP 15 through the Starter Dam at the toe in the central region of the dam but slightly closer to the right abutment, the following was observed:

- Drilling began at around 8:20 a.m. local time and proceeded until noon to a length of 83 m;

- Drilling resumed at 1:00 p.m. local time with casing installed to a length of 61 m;

- Drilling stopped between 2:00 p.m. and 4:30 p.m. local time, due to observed loss of pressure in the borehole as the hole crossed from berm fill to tailings;

- There was a loss of water recirculation in the borehole, under which condition the boring could not be advanced;

- Collapse of the borehole around the drill rod occurred and the drill rod was lost in the hole;

- There was mudflow (water with fines) from the borehole;

- Seepage and surface flows were noted from an area approximately 15 m towards the left abutment from the borehole and close to a nearby surface spillway channel;

- The hole was grouted with a cement mix, and casing was left in place; and

- Piezometric levels in nearby piezometers PZM-7 and PZM-9 rose by approximately 0.6 m and 3.5 m, respectively, shortly after the event; PZC-16 and PZC-24 also showed much lower increases in piezometric levels of approximately 0.3 m.

Following the DHP 15 incident, DHP installation activities ceased, and technicians worked for approximately three days to remediate the incident through the removal of water and use of sandbags. The area was monitored every 30 min, including overnight, until the piezometric water levels returned to normal, which occurred within several hours. A blocked pipe was identified and cleared near the location where DHP 15 was installed. Another blocked pipe was found approximately 20 m from the location of DHP 15; when this pipe was unclogged, the flows at DHP 15 significantly diminished, as did the flow at the pipe found near DHP 15. Within a few days, reports indicated that flows near the DHP 15 area significantly dropped. Following this incident, an inverted filter was installed at the location where surface flows were observed. No additional DHPs were installed following the DHP 15 incident.

The Panel's analysis of nearby seismograph records taken on June 11, 2018, showed low amplitude ground vibrations recorded around 1:36 p.m. local time (see Appendix I). These records had similar amplitude to the ground vibrations recorded just before the failure on January 25, 2019. However, it is uncertain whether these two events have a similar cause. The vibrations registered are extremely small and could be attributed to any number of events. Given what is known about the timing of the DHP incident, it is possible that the vibrations recorded on June 11, 2018, may reflect the local hydraulic fracture caused by DHP 15 along with some localized strength loss. The vibrations recorded on January 25, 2019, shortly before the visible failure likely also reflected a strength loss that could be associated with the internal initiation of failure.

4.4.3 Seepage

The design of Dam I included a system of lateral and subsurface drains, as described in Section 4.1.1. Flows from these drainage features were collected in surface drainage channels and pipes, and were monitored by means of flow meters, as discussed in Appendix C.

Seepage was observed and reported at various times through the history of Dam I. For example, seepage was reported from the surface of the Second Raising berm as early as 1983, and seepage was reported on the starter berm during the design of the Fourth Raising. Seepage was observed along the downstream slope near the toe of the Fourth Raising at the time of the design of the Ninth and Tenth Raisings in 2006.

Based on anecdotal reports, observed seepage was a regular occurrence on the lower portions of the downstream face of the dam since at least the construction of the Fourth Raising. However, annual technical safety audits of the dam conducted after the completion of the Tenth Raising generally do not identify seepage concerns until around 2018. A 2018 audit indicated seepage transitioning from "good practices" to "moderate noncompliance" beginning in early

2018.[10] In July 2018, a performance evaluation of Dam I indicated observance of moisture in the central section of the dam during construction of the surface water divergence system. The period from January 1, 2018 until the failure of the dam on January 25, 2019 identifies numerous instances of seepage and subsequent seepage mitigation efforts. However, interpretation of data from the same time period (including piezometric levels and flow meter data) do not suggest a change in conditions that could lead to an increase in seepage in the year prior to the failure. Accordingly, it is likely that the increase in seepage reporting during that time frame is attributable to changed reporting practices within Vale, rather than an actual increase in seepage.

4.4.4 Drilling Program Ongoing at Time of the Failure

At the time of the failure, two drilling campaigns were underway at the site. One of the drilling campaigns was the "As-Is" project, which was a subsurface exploration program that was intended to collect information on the material properties of the dam and natural ground. The second campaign was to install additional instrumentation in preparation for decommissioning of the dam. According to available records, as part of the "As-Is" project, eight boreholes were drilled between December 11, 2018, and the failure; one additional boring was in progress on the day of the failure (B1-SM-21). These boreholes were carried out just off the toe of the dam apparently to investigate the natural ground conditions in that region. As part of the instrumentation project, nine boreholes were completed prior to failure between October 2018 and the failure: four to install new inclinometers and five to install multiple electrical (vibrating wire) piezometers. Details are contained in Appendix A.

On the day of the failure, a tenth borehole (B1-SM-13) was being drilled at the central portion of the dam at the crest of the Eighth Raising to install new piezometers. No drill log or other driller's report is available for the activity taking place on January 25, 2019. According to available records, borehole BM-SM-13 was initiated on January 21, 2019, and on the day prior to the failure, drilling was reportedly advanced to a depth of 65.5 m below the ground elevation of approximately 929 m to a bottom elevation of approximately 863.5 m. This is the depth and elevation at which the drilling likely started on the day of the failure. Also, on the day prior to the failure, drilling was reportedly performed using rotary drilling methods with recirculation of water in the borehole, which is consistent with all other boreholes performed as part of this instrumentation drilling campaign. Below the water level, casing was used to support the borehole through the tailings. At the time of the failure, the drillers had been working for most of the morning and likely had advanced the borehole from the previous day's endpoint, possibly by as much as 15 m to a depth of approximately 80 m. Based on these depths, the borehole at the end of the previous day and on the day of the failure is expected to have reached natural ground. The previous nine boreholes were also drilled using the same method and extended through the tailings into natural ground. No signs of distress were reported during the other boreholes.

[10] Dam Technical Safety Report (ANM) (TÜV SÜD 2018) ("TÜV SÜD 2018 Technical Safety Audit ANM").

5 DEFORMATION OF DAM I PRIOR TO FAILURE

The Panel carried out a detailed analysis to determine if any deformations of Dam I occurred prior to the failure. Details of that analysis are contained in Appendix D. An integrated analysis was completed using available data, including topographic, survey, ground-based radar, satellite (InSAR), video, and drone.

There were 14 survey markers (prisms) located along the dam crest that were surveyed manually approximately once a month. A total of eight inclinometers were installed in the dam; six of these were active prior to the failure. Two inclinometers had data from May 2016 to December 2018, while the other four had been installed between October and November 2018 with only one reading taken in late December 2018. The two active inclinometers with data were read manually in two directions with readings taken approximately every other month (i.e., every 60 days). The survey and inclinometer systems were not able to detect small deformations, and no clear trends were detected above the measurement variations.

Ground-based radar data from Dam I were available from March 2018 to the time of the failure. The radar unit was installed in the stockpile area approximately 1,000 m from the dam face and collected data every three minutes (480 scans/day). The manufacturer's quoted precision is 3 mm/month (i.e., 36 mm/year). The radar deformation maps produced prior to the failure occasionally indicated large deformations of up to 700 mm/month. Upon review and re-analysis of the radar data, these are not true deformations but instead appear to be mainly the result of the radar's detection of "noise" due to the sensitivity of the radar to the presence of vegetation on the face of the dam, variable moisture retained in the vegetation and soil, humidity in the atmosphere, and the rapid scanning frequency, which did not facilitate filtering of the noise. The radar data were analyzed along the concrete surface drains on the downstream face of the dam, which were not influenced by vegetation, and these showed no detectable deformations. The radar data also were reviewed through a "slow movement" analysis using one image every 24 hours. Such review has the potential to reduce the noise level, thereby allowing a more accurate interpretation. The "slow movement" analyses did not detect any significant deformations along the radar line-of-sight (LOS) during the period from March 2018 through December 2018.

Small, rapid deformations were recorded by the radar on June 11, 2018, in the central part of Dam I, approximately 35 m and 55 m above DHP 15 following its installation. Because these deformations were rapid and occurred in a relatively short period of time, the detected deformations are considered reliable. Closer to DHP 15, initial positive (outward) deformations of up to 6.4 mm were recorded, with an average deformation of 2.4 mm, followed by negative (inward) deformations of up to 14.1 mm, with an average of 3.9 mm. Further from DHP 15, only positive deformations were recorded, up to a maximum of 8.3 mm, with an average of 3.6 mm. What made the radar's recording of these deformations more reliable is that they occurred relatively rapidly, which reduces the noise effects.

In January 2019, small deformations were detected by the radar in the lower part of the dam toward the left abutment, but these were too close to the minimum detectable velocity of the

radar to be confirmed as actual deformation. In addition, these deformations reported by the radar do not correlate with those reported by satellite InSAR (discussed below). Under the conditions prevailing at the site, such as vegetated surfaces, humid climates, and equipment operating and processing procedures, the ground-based radar was unable to detect small slow deformations on the dam.

The Panel obtained and used InSAR data to evaluate deformations of the dam and impounded tailings in the one-year period prior to failure. The InSAR images provide about an order of magnitude higher precision than the ground-based radar, since the radar wavelength used for InSAR is longer, making the results less sensitive to moisture, and hence generating less noise. The analysis of the InSAR data indicates small downward deformations near the crest and mid-height of the dam of no more than 30 mm/year. In the lower parts of the dam in the central region, the analysis indicates small deformations of up to 36 mm/year, mostly in the downward direction. Figure 20 shows the quarterly velocities of deformation in the 12 months before the failure in the central region of the dam. It also shows that the deformations near the crest are mostly vertical, while closer to the toe of the dam the deformations have a slight horizontal outwards component. The horizontal deformations (in the east-west (E-W) direction) near the toe of the dam were mostly less than 10 mm/year over that period, but included some small areas with up to 30 mm/year. The deformation vectors inferred from InSAR do not include the north-south (N-S) component since the LOS of both ascending and descending orbits were almost perpendicular to that direction and, hence, likely to be an unreliable estimate of the actual deformations. A comparison between the InSAR and rainfall data indicates a correlation where deformations tend to increase slightly during the wet season. The observed deformations from the InSAR were too small and slow to be reliably detected by the survey, inclinometers, and ground-based radar methods used. The CPTu data show that the tailings within the dam were fully consolidated. Hence, such deformations in the dam are consistent with slow, long-term settlement of the dam, likely the result of ongoing internal creep, and are not indicative of a precursor to failure.

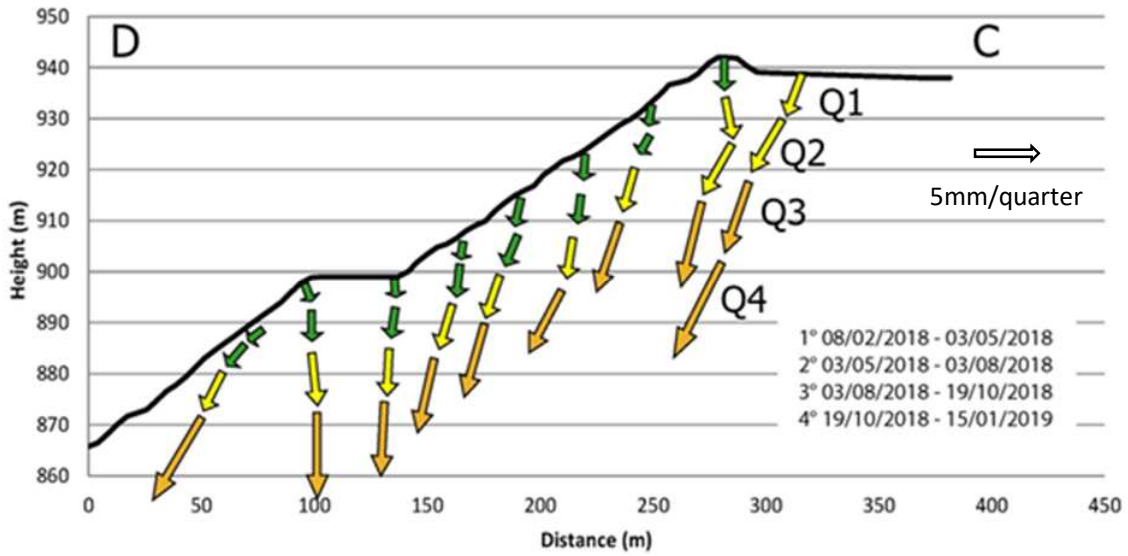

Figure 20: Cross-section Showing Deformation Vectors for the Four Quarters Prior to Failure

Larger vertical deformations, to a maximum of 140 mm/year, were detected in the tailings impoundment. Based on the data available, it is difficult to separate ongoing settlement of the tailings due to consolidation of the softer, finer tailings far behind the dam from deformation of the dam. However, because the settlements were mostly vertical and were well back from the crest, it is likely they were predominantly the result of long-term consolidation.

High-quality video images of the dam from a drone flown seven days prior to the failure show no signs of distress and no indications of excessive seepage.

6 MATERIAL CHARACTERIZATION

Several major geotechnical studies were carried out between 2005 and 2019 to characterize the materials within the dam. These studies included drilling, sampling, CPTu, FVT, and Vs measurements, and installation of additional instruments. Laboratory testing was also carried out on samples. Details are contained in Appendix B.

The historical data were supplemented with field investigations and advanced laboratory testing carried out by the Panel after the failure. The combined data provide a clear picture of the distribution, behavior, and consistency of the material in the dam before the failure. The objective was to determine parameters from the field and laboratory data to perform deformation and stability analyses intended to simulate the conditions prior to the failure and to test potential failure trigger mechanisms. The following sections describe the main conclusions obtained from the historical data and the data obtained by the Panel.

6.1 Historical Data

6.1.1 Field

Major geotechnical investigations were carried out between 2005 and 2019. A significant part of these investigations was a series of CPTu that provide a detailed profile of subsurface conditions. The CPTu performed in 2005 were generally to shallow depth due to limitations in pushing equipment. However, the CPTu performed in 2016 and 2018 were of good quality and often extended the full depth of the tailings. The 2016 and 2018 CPTu also included numerous dissipation tests that provide insight regarding soil type and equilibrium water pressure profiles. Figure 21 shows the layout of the CPTu on the dam and the main cross-sections and longitudinal sections used in this study.

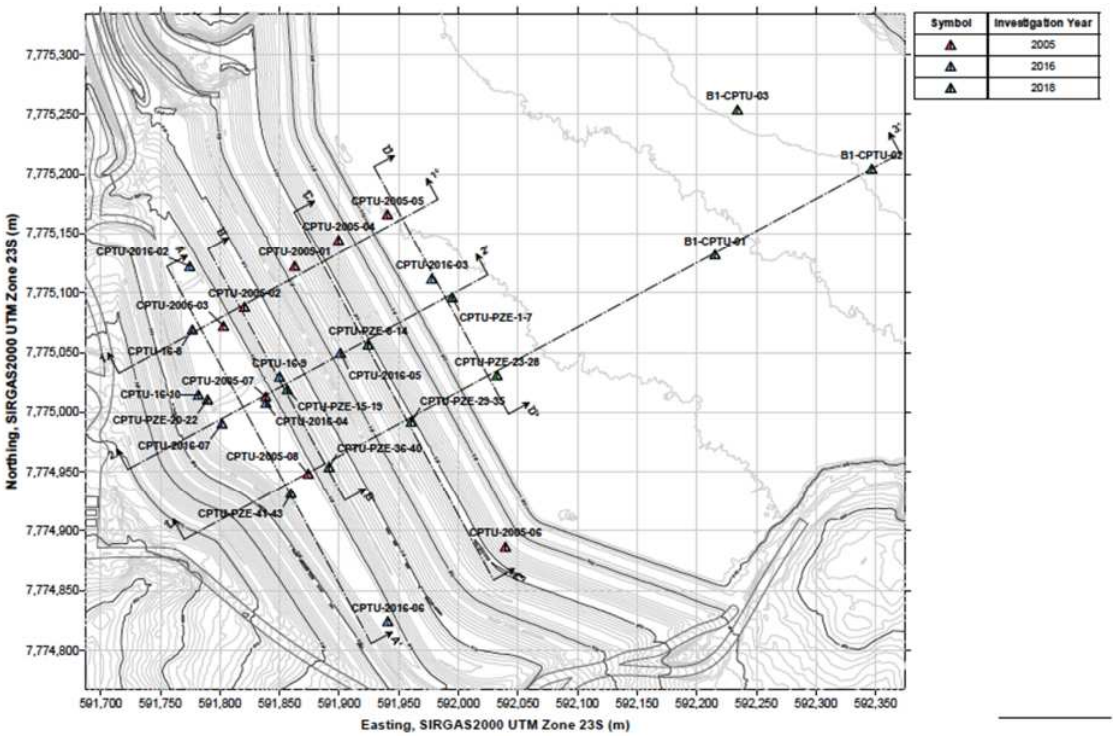

Figure 21: Layout of CPTu Carried Out in 2005, 2016, and 2018

The concept of upstream construction is to form a free-draining beach of more coarse-grained tailings with finer tailings deposited further from the crest and slimes deposited in the pond region. It is clear from aerial photos and satellite images that beach lengths varied considerably over the life of the dam and that more fine-grained tailings were deposited close to the previous crest locations, resulting in layers of fine tailings under the dam. The CPTu profiles confirm this and show that the materials under the dam were composed of interlayered coarse and fine tailings. Figure 22 shows an example CPTu profile (PZE-29-35) from the central portion of the dam performed at the top of the Eighth Raising during the 2018 program. This profile extends almost the full height of the dam and appears to penetrate natural ground at about an

elevation of 872 m msl. The CPTu shown in Figure 22 illustrates the predominately coarse tailings with thin layers of fine tailings.

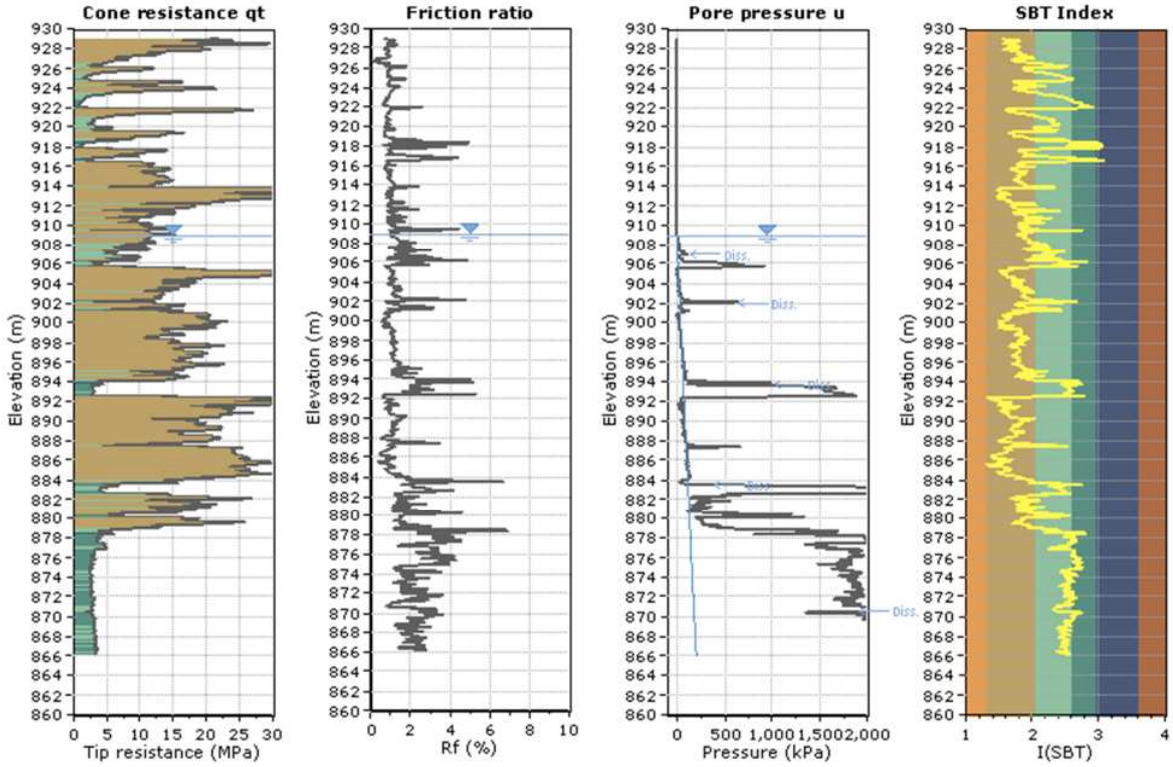

Figure 22: Example CPTu Profile for PZE-29-35

To understand the distribution of the tailings, the materials were grouped by regions with similar material strengths and CPTu behavior types. Generally, it was observed that the coarse tailings had a lower apparent fines content[11] and a material index (I_c) of less than 2.6, whereas the fine tailings layers were observed to have a higher apparent fines content and an I_c greater than 2.6.

The CPTu indicate that water levels were generally high, especially in the lower regions of the dam; the coarse tailings are essentially free draining during the CPTu; and the fine tailings are essentially undrained during the CPTu. Dissipation tests had been carried out predominately in the fine tailings and show that dissipation rates were relatively rapid (e.g., time for 50% dissipation, t_{50} < 400sec) and that the resulting equilibrium pore pressures show a downward gradient. On average, the downward gradient produced a water pressure profile that is about 50% of the hydrostatic water pressure profile. The relatively rapid CPTu dissipation rates indicate that the fine tailings are composed of predominately silt-size particles. The tailings

[11] Based on Robertson, P.K., & Wride, C.E. (1998). Evaluating cyclic liquefaction potential using the cone penetration test. *Canadian Geotechnical Journal, 35,* 442-459.

appear to be saturated below the water level with a continuous hydraulic gradient. No perched water levels were detected.

Two CPTu (B1-CPTu-02 and -03) were carried out in 2018 in the pond region through slimes and show that the slimes are a relatively homogenous, very soft, essentially normally consolidated clay-like material. The dissipation tests in the slimes indicate that they were essentially fully consolidated with no excess pore pressures. The measured t_{50} values in the slimes were considerably longer (t_{50} > 1,000 s) than those recorded in the fine-grained tailings under the dam. One CPTu was carried out approximately midway between the pond and the crest (B1-CPTU-01) and showed interlayered coarse and fine tailings overlying slimes. The dissipation times (t_{50}) in the fine tailings were similar to those recorded in the fine tailings in the dam.

The CPTu results indicate that the tailings are predominately loose and contractive at large strains, consistent with other hydraulically deposited tailings. Figure 23 shows an example CPTu (PZE-29-35) on the modified soil behavior type chart[12] to illustrate that the tailings below the water level (in this case, those collected between elevation 910 m msl to 878 m msl) are contractive at large strains. The CPTu data shown in Figure 23 were normalized using an appropriate high unit weight for the tailings and the measured downward piezometric gradient.

[12] Robertson, P.K. (2016). Cone penetration test (CPT) based soil behaviour type (SBT) classification system – an update. *Canadian Geotechnical Journal*, *53*(12), 1910-1927.

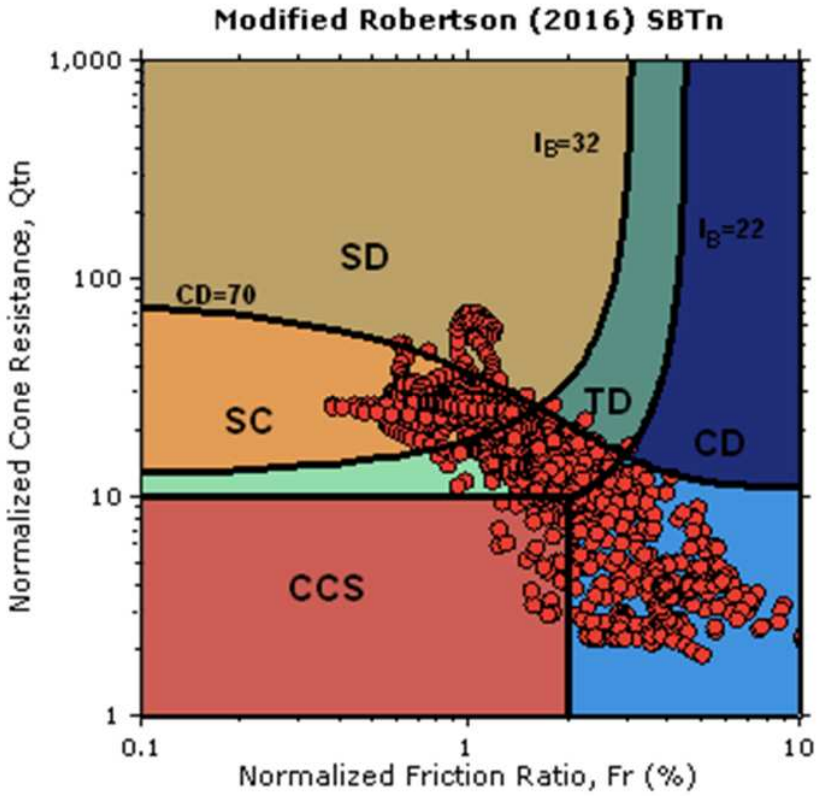

Figure 23: Example CPTu (PZE-29-35, from Elevation 910 m msl to 878 m msl)

FVTs were carried out in 2005 and 2016 predominantly in fine tailings layers. Due to the relatively high permeability of the fine tailings, the results of the FVTs were likely influenced to some degree by partial drainage and are less likely to provide reliable estimates of undrained strength. Although the individual strength values obtained from the FVTs may not be reliable, the results consistently showed trends of significant and rapid strength loss in the tailings tested.

The previous investigations also included a small number of Vs measurements with depth. When the Vs measurements are combined with the adjacent CPTu data, there is an indication of slight microstructure (based on the approach by Robertson, 2016). Given the young geologic age of the tailings (< 37 years), the microstructure is likely due to a small amount of bonding. This bonding appears to be more prevalent in the fine tailings. Typically, CPTu measurements reflect the soil behavior at large strains after any bonding has been destroyed, whereas Vs measurements reflect the stiffness of the soil at very small strains, which tend to be dominated by the bond strength.

6.1.2 Laboratory

Previous geotechnical investigations provide a detailed summary of basic index test results, as summarized in Appendix B. The coarse tailings have a fines content (based on 0.075 mm sieve size) between 20% and 50%, and are non-plastic. The fine tailings under the dam have a fines

content between 50% and 90% with a low plasticity (average Plasticity Index (PI) of 10%). The historical data also show that the total unit weight of the tailings is generally high with an average value of around 26 kN/m^3. The associated specific gravity also is high with an average value of around 4.5. The historical records have some mineralogical data, and testing carried out in 2006 indicate a high iron (total ferrous) content (> 50%) and low quartz (silica) content (< 10%).

During the 2005 investigation, a series of intact samples were obtained at shallow depth on the beach using careful block and tube sampling. The block samples had an average *in situ* void ratio of 1.0. This high average void ratio measured from block sampling supports the interpretation that the tailings were generally loose. A void ratio of 1.0 shows that approximately 50% of the total volume of tailings was composed of void space. Since much of the void space is filled with water, the high void ratio shows that a significant portion of the tailings was water. Since the total volume of tailings was about 12 Mm^3, it is reasonable to assume that the total volume of water stored in the tailings was up to 5 Mm^3 (given that some tailings were unsaturated above the water level). This volume of water is approximately equivalent to about 2,000 Olympic size swimming pools of water. Since the region has high rainfall, dewatering the stored tailings would be challenging and slow.

The historical triaxial strength testing shows significant variability in material behavior. Some tests carried out on intact samples indicate a very brittle response.

6.2 Material Distribution

Based on the previous site investigation data, combined with analyses of past aerial and satellite images, it is possible to recreate detailed cross-sections of the stratigraphy under the dam. Details are contained in Appendix F.

Figure 24 shows an example of a recreated cross-section for the steepest and highest section of the dam (cross-section 3-3). Figure 24 shows that the predominate material under the dam was coarse tailings (shown in yellow) with thin layers of fine tailings (shown in orange). In general, the tailings become more fine-grained with depth, reflecting the increasing distance from past crest elevations during the upstream construction. The slimes (shown in red) are generally farthest from the Dam.

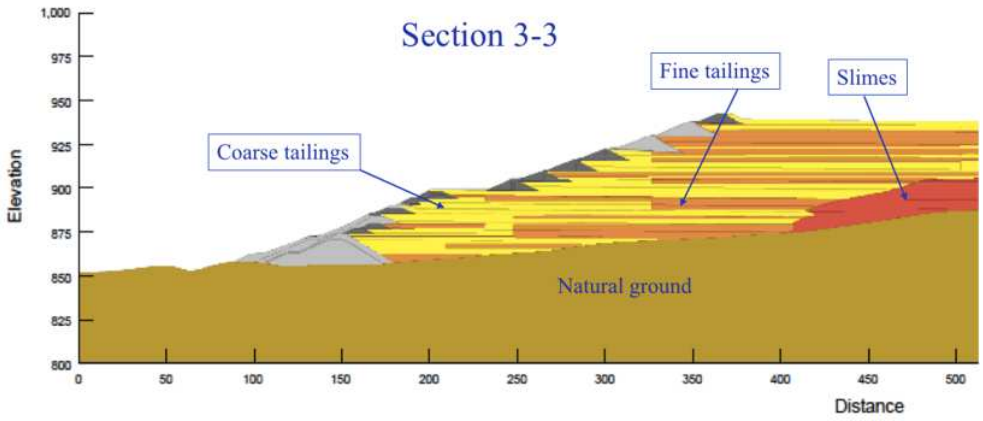

Figure 24: Recreated Cross-section 3-3 Based on Historical Data, Expanded to Show Details Under the Dam

6.3 Field Studies by the Panel

Two members of the Panel visited the site on March 28, 2019, to make initial observations. The site visit included a helicopter view of the failure and surrounding mine site, and a walk-over from the right abutment (the left abutment was not accessible) to evaluate access for future field investigations. Helicopter views of the failure are shown in Figures 25 and 26.

Figure 25: Aerial View of Failed Dam I, Looking Approximately South-East, Photographed on March 28, 2019

Figure 26: Aerial View of Failed Dam I, Looking North, Photographed on March 28, 2019

All four Panel members visited the site on June 4, 2019, to make further observations and to collect representative bulk samples. Although the samples were collected after the failure, they were collected from various locations at the dam site to represent the different materials that would have been found within the dam. The locations selected were based on accessibility, visual observations, and knowledge of construction history. In addition, laboratory testing by the Panel, discussed below, confirmed the representative nature of the samples because the results of the testing were consistent with available pre-failure geotechnical and mineralogical testing. Further information on the sampling method employed by the Panel can be found in Appendix E, and details of the pre-failure investigations are discussed in Section 6.1 and are further detailed in Appendix B.

The bulk samples of coarse tailings were taken from exposed surfaces of intact tailings that represent beach tailings from previous raises below the final dam, as shown on Figure 27. The samples were obtained from an exposure that was estimated to be below the Seventh Raising at the right abutment. Figure 28 shows the distinct thin layering in the coarse tailings sample locations.

Figure 27: Sample Locations from June 2019 on Post-failure Image

Figure 28: Coarse Tailings Sample Locations S6a (Left) and S6b (Right)

A more detailed field program was carried out July 1-23, 2019, to address gaps in the data that included the following:

- Guelph permeameter tests to measure infiltration characteristics;
- Tensiometer readings of matric suction near the surface;
- Sand-replacement density tests adjacent to the permeameter tests;

- Surface flow measurements to estimate flow rates from post-failure springs; and
- Boreholes (with sampling) of foundation soils.

Test locations are shown in Figure 29.

Figure 29: Google Earth Image Showing Test Locations for the July 2019 Field Program

GP	Guelph permeameter tests
DT	Sand replacement density tests
FL	Surface flow measurements
BH	Boreholes in natural ground

Details of both field programs are contained in Appendix E.

Four boreholes were carried out in July 2019 to obtain information about the natural ground within the dam's foundation. The boreholes showed that the natural ground is composed of residual soils. It was not possible to differentiate between colluvium and residual soil. The residual soil encountered in the boreholes was described as stiff to very stiff with evidence of residual bonding from the parent bedrock that is primarily gneiss. The boreholes show no evidence of continuous weak layers within the natural soils encountered.

6.4 Laboratory Studies by the Panel

Details and results of the laboratory testing carried out by the Panel are contained in Appendix E.

A series of index tests was carried out on the samples obtained by the Panel from the 2019 field programs with the objectives of: (i) characterizing the materials; (ii) comparing the data with pre-failure historical data; and (iii) confirming the representativeness of the samples.

The index testing confirmed that the coarse tailings are poorly graded and have a fines content (based on 0.075 mm sieve size) between 20% and 50%, and are non-plastic. The fine tailings under the dam have a fines content between 50% and 90%. The slimes are more well graded with essentially 100% fines content and PI of around 18%. Figure 30 shows a comparison between the coarse tailings particle size distribution curves collected in 2019 and some historical curves, and shows that the 2019 samples are similar to historical samples collected under the pre-failure dam.

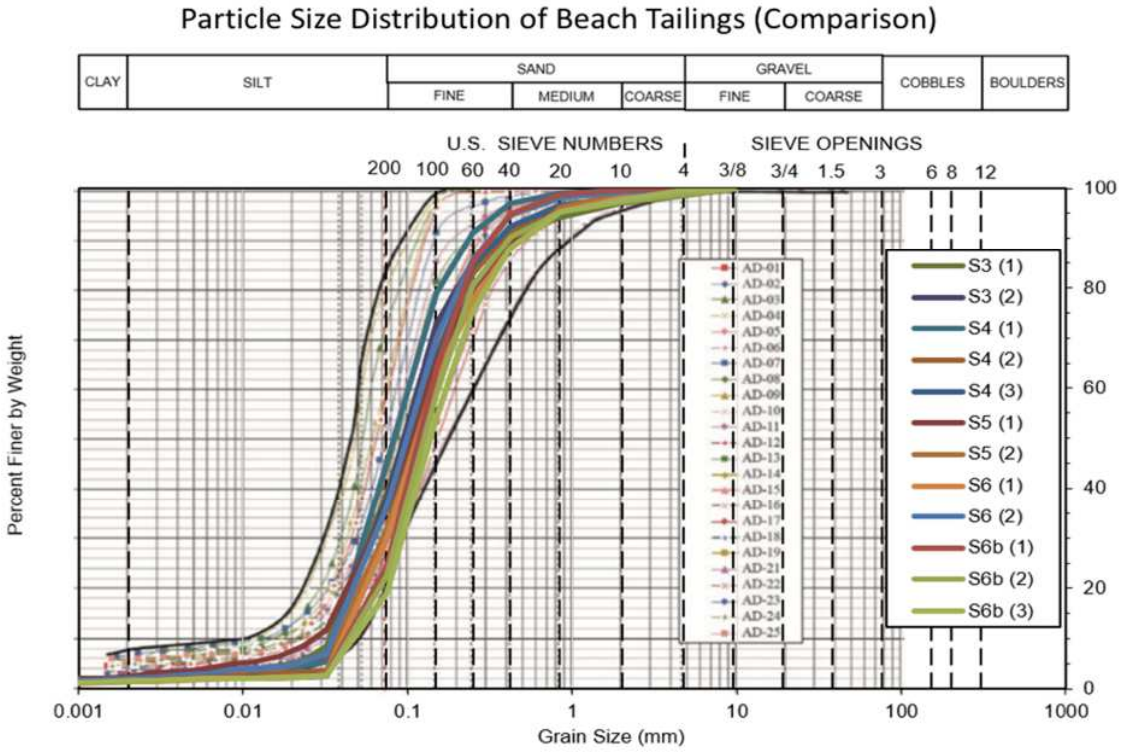

Figure 30: Comparison of Particle Size Distribution Curves from the 2019 Samples with Pre-failure Historical Data

Testing on the 2019 samples show that the specific gravity is around 4.9 for the coarse tailings and closer to 4.0 for the slimes. The natural residual soil has a more traditional specific gravity of around 2.75. The high specific gravity in the tailings produces a high soil unit weight for the tailings of around 26 kN/m^3.

X-ray diffraction (XRD) testing was carried on several 2019 tailings samples and showed high contents of iron (combined hematite, goethite, and magnetite). The coarse tailings samples obtained in June 2019 were obtained from an area under the Seventh Raising, whereas the samples obtained in July 2019 were obtained from the surface tailings very close to the

abutments. Higher goethite was measured in the surface samples, which indicated increased weathering and oxidation of the iron. In summary, the total iron content (combined hematite, goethite, and magnetite) for the tailings in the dam was high (greater than 50%) with a small quartz content of generally less than 10%. These values are consistent with historical data on the tailings obtained in 2006, as detailed in Appendix B.

This mineralogy is significantly different from most natural soils that are predominately composed of quartz (i.e., silica-based minerals). The mineralogy also is significantly different from the soils used to develop the traditional empirical correlations used to interpret *in situ* tests, such as the CPTu, which would indicate that these empirical correlations may not provide reliable results in these tailings.

Table 2: XRD Results – June 2019 Samples

Mineral	Ideal Formula	# 1 Sample 1 Bag 2 X-ray (Slimes)	# 2 Sample 1 Bag 4 X-ray (Slimes)	# 3 Sample 3 Bag 2 X-ray (Coarse Tailings)	# 4 Sample 5 Bag 1 X-ray (Coarse Tailings)
Hematite	α-Fe_2O_3	50.1	44.4	87.7	86.8
Goethite	A-$Fe^{3+}O(OH)$	32.0	34.0	3.4	3.0
Magnetite	Fe_3O_4	0.4	0.4	6.5	7.6
Quartz	SiO_2	5.4	6.6	1.6	1.5
Kaolinite	$Al_2Si_2O_5(OH)_4$	6.2	8.9	0.6	0.6
Talc	$Mg_3Si_4O_{10}(OH)_2$	2.7	2.3	-	-
Gibbsite	$Al(OH)_3$	0.9	1.0	0.3	0.4
Bayerite	$Al(OH)_3$	2.2	2.4	-	-
Total		100.0	100.0	100.0	100.0

Table 3: XRD Results – July 2019

Mineral	Ideal Formula	DT-01 (Slimes)	DT-02 (Slimes)	DT-06 (Fine Tailings)	DT10 (Fine Tailings)
Hematite	α-Fe_2O_3	43.1	54.1	50.3	44.3
Goethite	A-$Fe^{3+}O(OH)$	20.7	15.3	10.2	13.7
Magnetite	Fe_3O_4	1.9	1.5	1.3	1.3
Quartz	SiO_2	14.9	12	28.5	21.8
Kaolinite	$Al_2Si_2O_5(OH)_4$	11.6	10.9	6.4	13.5
Talc	$Mg_3Si_4O_{10}(OH)_2$	3.1	2	1.4	1.1
Gibbsite	$Al(OH)_3$	3	2.2	1.4	3
Bayerite	$Al(OH)_3$	1.7	2	0.5	1.4
Total		100.0	100.0	100.0	100.0

Scanning electron microscope (SEM) images were taken of samples of coarse tailings and slimes from the June 2019 field program to qualitatively assess particle structure, angularity, and other parameters at the microscopic level. Example images are shown in Figures 31 (coarse tailings) and 32 (slimes). The SEM images confirm the high iron content and show that the particle shape is similar for both materials and that the grains are typically sub-angular to angular with rough, often pitted surfaces. Additional SEM images were taken to study the interaction between particles and showed evidence of bonding between particles, shown in Figures 33 and 34. The nodules shown in Figure 33, and highlighted in Figure 34, are composed of iron oxide. The bonding appears to be derived from clay-size iron oxide. It appears that oxidation of the iron produces bonding between particles.

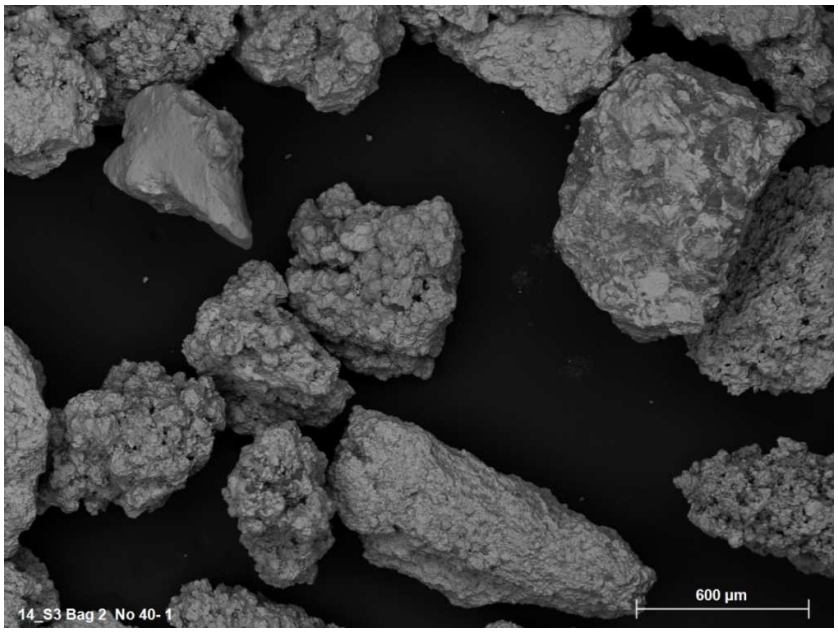

Figure 31: SEM Image of Sample 3 Bag 2 – Coarse Tailings

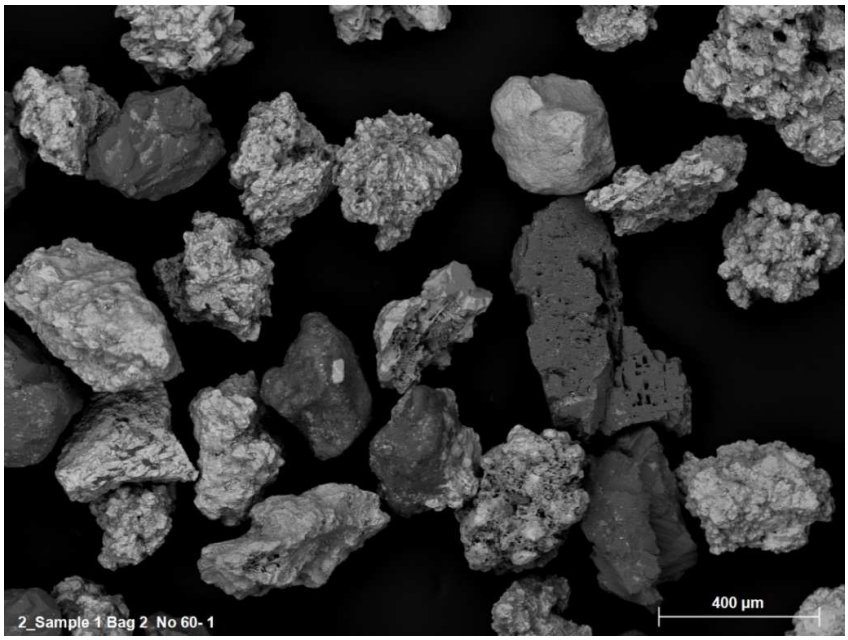

Figure 32: SEM Image of Sample 1 Bag 2 – Slimes

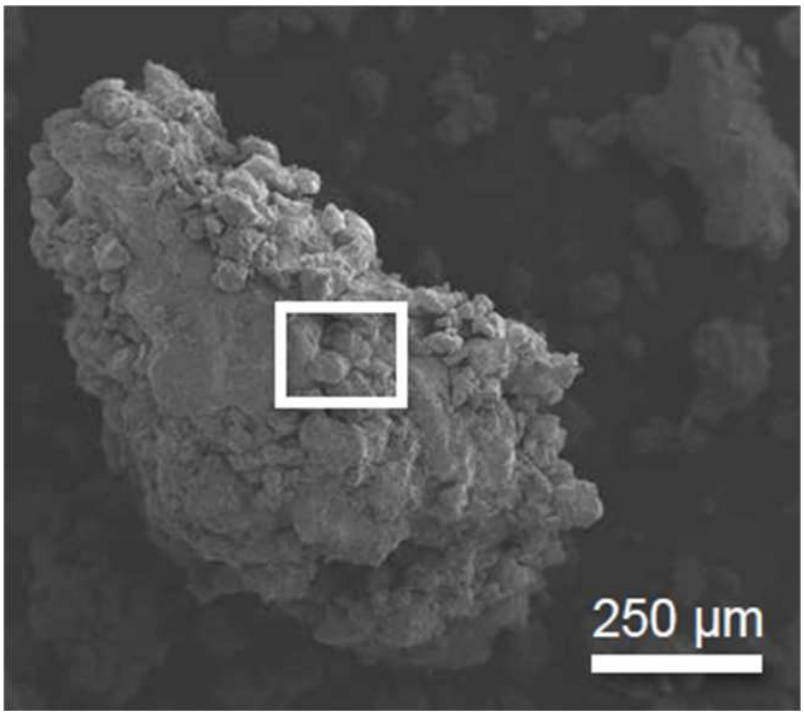

Figure 33: SEM Image of Coarse Tailings

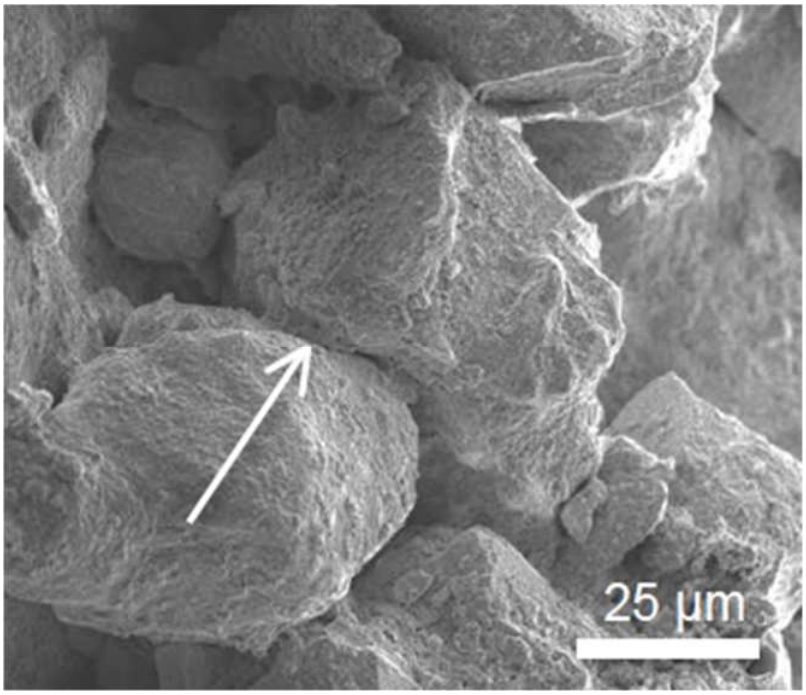

Figure 34: SEM Image of Coarse Tailings (Detail of Box Shown in Figure 33). Region Highlighted with Arrow Shows Bonding Between Particles

6.5 Advanced Laboratory Testing by the Panel

This section describes the main observations made from advanced laboratory testing performed on samples of representative tailings that were sieved to form consistent reference samples of coarse and fine tailings for laboratory testing. Details of the testing are contained in Appendix E. Reference samples were reconstituted in the laboratory to densities (void ratio) that were similar to those in the dam, since undisturbed intact samples were not available.

The Panel elected to run advanced computer modeling using a Critical State (CS) framework. Hence, one of the objectives for the advanced laboratory testing was to determine CS parameters. Since undisturbed intact samples of the pre-failure tailings were not available, testing was carried out on reconstituted samples. Due to the potential impact of fines on the CS parameters, bulk samples were created using the June 2019 samples to generate representative gradations. The average and range of gradation of the tailings from historical laboratory test data were used to establish representative gradations. Representative samples were established to match the average, coarse, and fine tailings gradations from historical laboratory testing. Figure 35 summarizes the representative gradations.

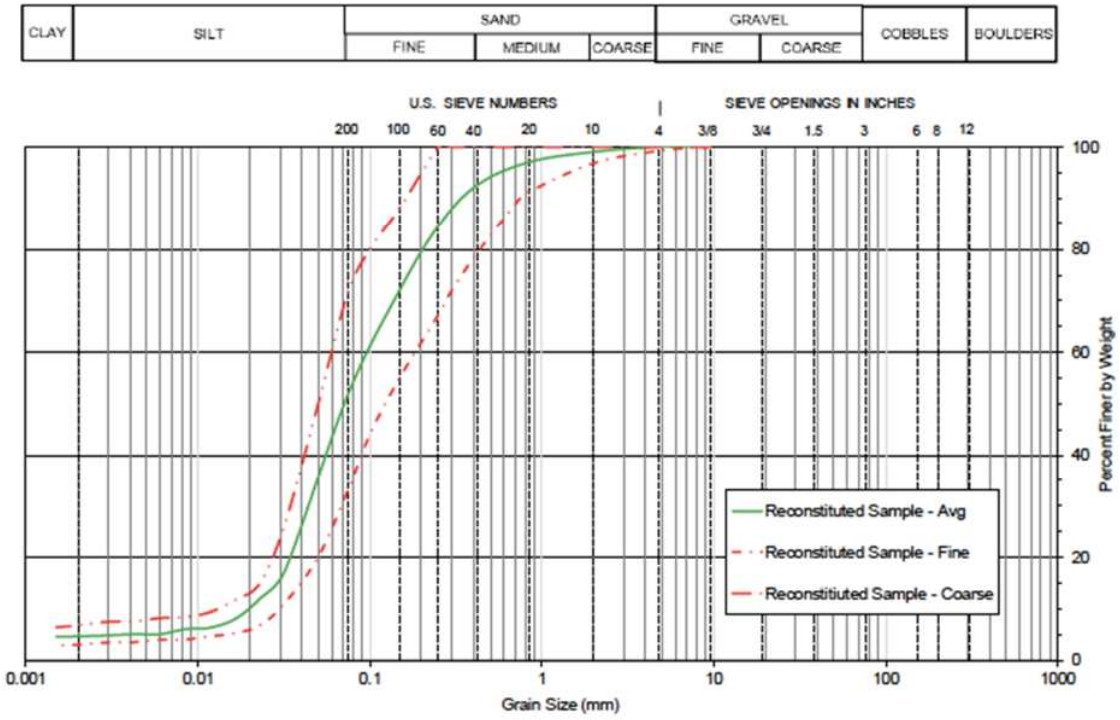

Figure 35: Gradations Constructed to Represent Average, Coarse, and Fine Gradations for Testing

Samples were prepared by moist tamping in general accordance with procedures outlined by Jefferies and Benn (2016). Because the intact tailings observed after the failure showed clear signs of very thin layering, the Panel considered that moist tamping could duplicate the thin horizontal layer as well as provide excellent control on target densities and void ratios.

Advanced laboratory testing included standard strain-controlled triaxial tests as well as load-controlled triaxial tests using dead weights. Tests were carried out drained and undrained, as well as isotropically and anisotropically consolidated.

The main observations from the advanced laboratory testing are summarized below.

- The Critical State Lines (CSLs) for the average, coarse, and fine gradations are very similar in shape and slope, but the fine tailings have slightly higher void ratio.
- The triaxial data show an unusual response during shear:
    - Loose samples develop a peak friction angle greater than the CS friction angle (ϕ'_{cs}); and
    - Dense samples developed a greater amount of dilatancy than typical for other tailings and natural soils.
- The high dilatancy produces a very steep stress-strain curve with a peak strength that is higher than estimated from empirical relationships and a residual (or liquefied) strength that is lower than implied by empirical relationships.
- The axial strain required to reach peak strength is very small (< 1%).
- A rapid strength loss (i.e., brittle response) is observed in both drained (dense samples) and undrained (loose samples) tests.
- The high peak strength and brittle response appear to be a reflection of light bonding.

A series of undrained triaxial tests was carried out to determine the relationships between the pre-test state and peak and liquefied undrained strength ratio, as well as the strains to reach these strengths. These tests showed a clear relationship with the pre-test state and showed that the strains required to reach peak strength were very small for loose samples and became larger with increasing density. The results also showed that denser samples had very high undrained peak strengths due to bonding. These main observations are illustrated in the following figures.

The shape and location of the CSLs, shown in Figure 36, are consistent with the similar grain characteristics (shape, angularity) and mineralogy of the tailings tested, even though the mean particle size varies. The ϕ'_{cs} for each gradation was also very similar with an average value of 34 degrees.

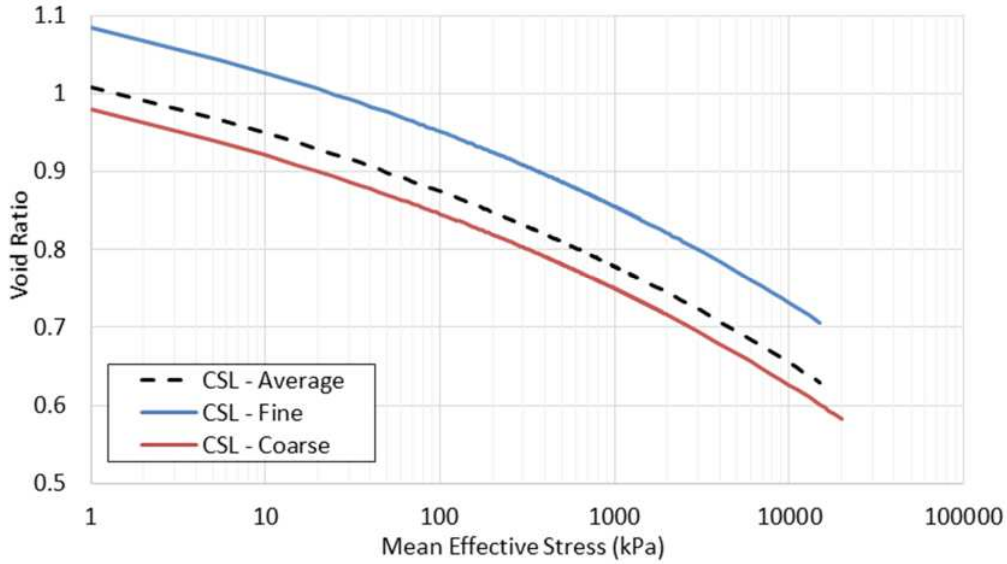

Figure 36: Comparison of CSLs for the Representative Tailings Tested

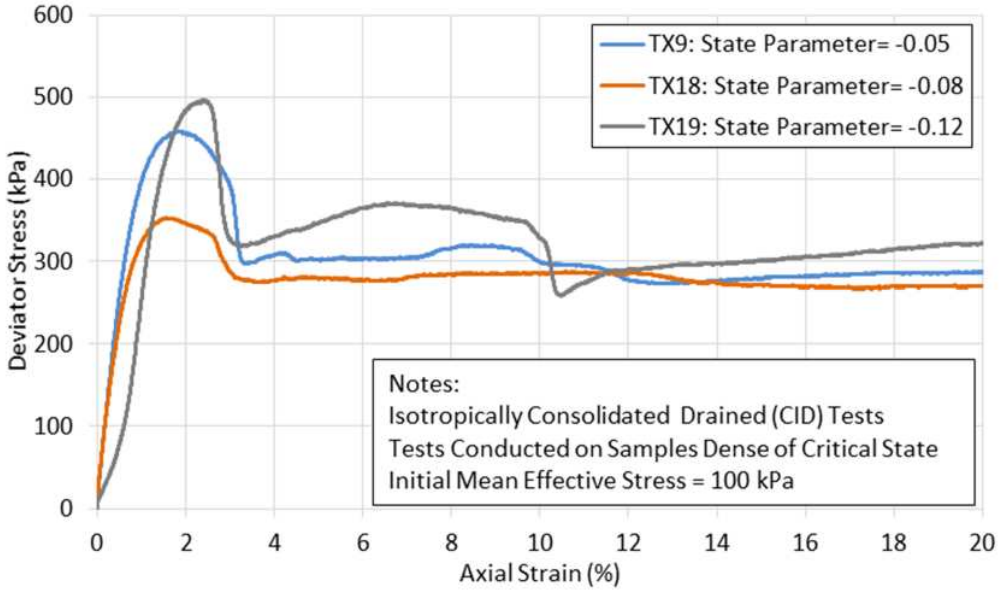

Figure 37: Comparison of Isotropically Consolidated Drained Triaxial Tests on Average Gradation Samples at Different State Parameters that are Dense of CS

Figure 37 compares the results of isotropically consolidated drained (CID) triaxial tests on average gradation samples consolidated to the same effective stress (100 kPa) but prepared to different state parameter (ψ) values (void ratio) that are dense of CS. The rapid strength loss and the peak strength is inconsistent with the state (void ratio) of the samples (e.g., the looser state (ψ = -0.05) has a similar peak strength as the densest state (ψ = -0.12)).

Figure 38 shows the test result of a CID triaxial test on an average gradation sample consolidated to 50 kPa and prepared to a state that is loose of CS (ψ = +0.09). For a sample that is loose of CS, the expected behavior would be for the sample to show a gradual increase in deviator stress (q) combined with a gradual decrease in volume to CS. However, this test showed a very stiff response to peak q at an axial strain of about 1%, followed by an abrupt reduction (collapse) in volume at a constant mean effective stress (p') and q.

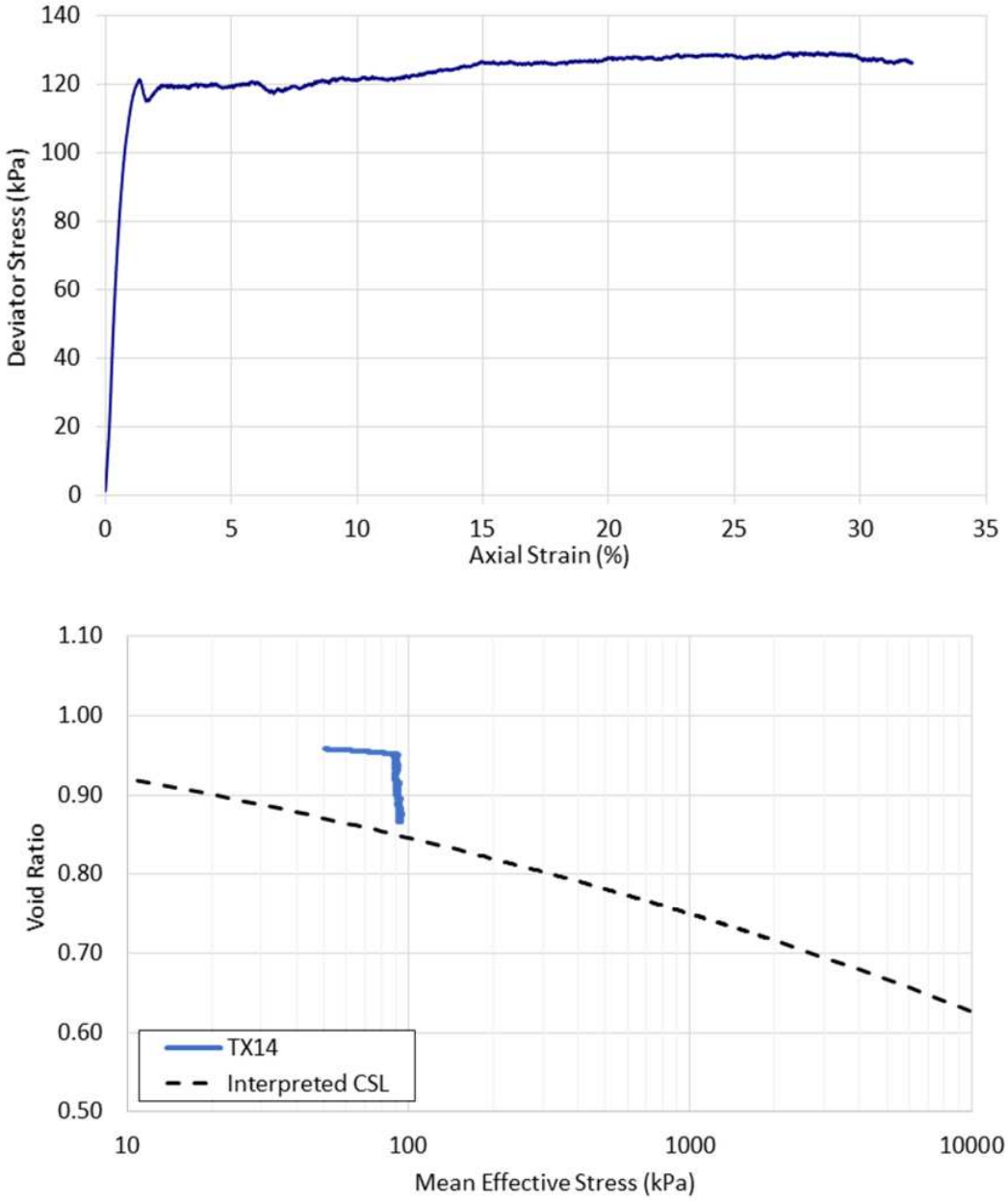

Figure 38: CID Triaxial Test Result on an Average Gradation Sample Consolidated to 50 kPa Prepared to a State Loose of CS (ψ = +0.09)

One aniostropically consolidated undrained (CAU) triaxial test was performed on fine and coarse gradations to assess the undrained response of a loose sample of these gradations to identify whether they are similar. Both samples were anisotropically consolidated to a mean effective stress of 200 kPa and a ratio of horizontal to vertical effective stress, K_0, of 0.5 before starting the undrained loading. The fine and coarse samples were prepared to the same state parameter of ψ = +0.07. The results of these tests appear in Figure 39, which shows that both samples generated an extremely brittle response during the undrained loading. The samples failed at 0.3% and 0.8% axial strain for the fine and coarse gradations, respectively. The peak strength ratios ($s_{u(peak)}/p'$) for the fine and coarse gradation samples were 0.42 to 0.51, respectively (equivalent to $s_{u(peak)}/\sigma'_v$ = 0.26 and 0.34). The residual strength ratios ($s_{u(residual)}/p'$) for the fine and coarse gradation samples were 0.005 to 0.01, respectively. These peak strength ratios are significantly higher than empirical estimates based on CPTu data, such as those of Olson and Stark (2002), and the residual (or liquefied) strength ratios are significantly lower than empirical estimates, such as those of Robertson (2010). The test results also confirmed that the fine and coarse gradations behave in a similar manner during undrained shear.

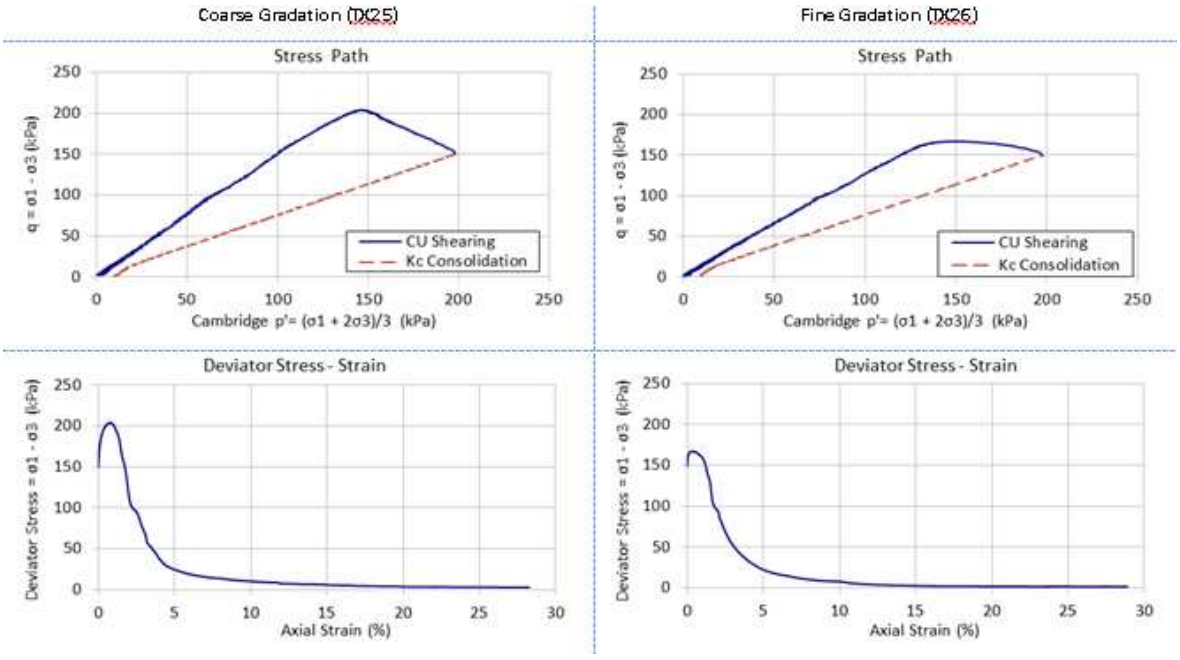

Figure 39: Results of CAU (K_0 = 0.5) Strain-controlled Triaxial Tests (Coarse and Fine Gradations)

Two triaxial load-controlled tests using dead loads (TXDW) were completed for comparison with the strain-controlled tests. Both tests were completed on the coarse gradation sample. The first test (TXDW01) was completed as a drained test and was intended to replicate test TX14, which was a strain-controlled CID test carried out at an initial *p'* of 50 kPa and a state parameter of +0.09 (Figure 40). The CID test (TX14) showed an abrupt reduction in volume at around 1% strain, at a constant *p'* and *q*. The purpose of the equivalent load-controlled test (TXDW01) was to see if this volumetric reduction would lead to pore pressure generation and

strength loss under dead load conditions. The equivalent dead load test was anisotropically consolidated to stresses approaching those at which TX14 failed; however, the sample failed in a rapid manner at smaller stresses. The rapid nature of the failure indicates it occurred undrained. The load-controlled test also showed significant creep under constant *q*.

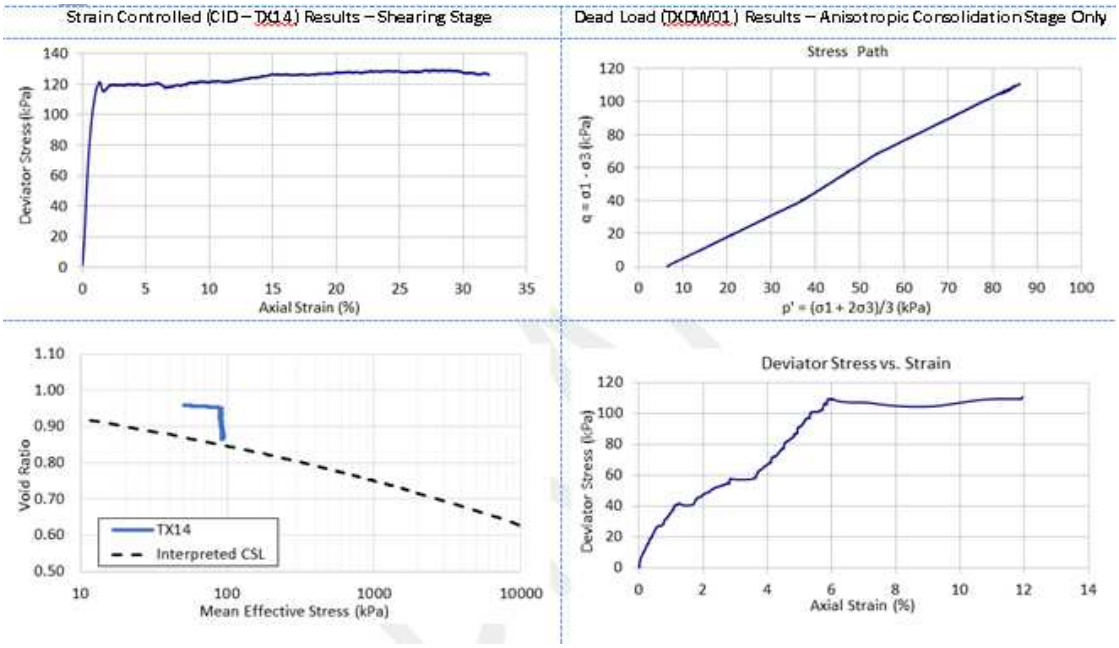

Figure 40: Comparison Between an Isotropically Consolidated Strain-controlled Test (CID-TX14) and Anisotropically Consolidated Load-controlled Test (TXDW01) with the Same State (ψ = +0.09) and Coarse Gradation

The second dead load test (TXDW02) was carried out for comparison with the anisotropically consolidated strain-controlled undrained (CAU) test (TX25) completed at an initial *p'* of 200 kPa and a K_0 of 0.5, as shown in Figure 41. Except for the dead weight load application, TXDW02 was completed in exactly the same manner as TX25. The load-controlled test (TXDW02) failed at an axial strain of 0.7% and a peak undrained shear strength ratio of 0.55. The residual (liquefied) strength ratio of this sample could not be measured because the failure occurred in a rapid manner and produced complete failure of the sample. The brittle response, peak undrained shear strength ratio, and small strain to peak were similar for both tests, illustrating general consistency across testing methods.

Bender element testing also was carried out on several isotropically consolidated triaxial samples to evaluate the relationship between normalized shear wave velocity (V_{s1}) and void ratio (*e*); details of this testing are contained in Appendix E. This testing showed a relationship between V_{s1} and *e*, but there was very little change in V_{s1} for a significant change in *e*. This observation is supportive of slight bonding.

Direct simple shear testing was conducted on selected samples of the natural foundation residual soils obtained from the 2019 drilling campaign. Details are presented in Appendix E.

The results indicate that the residual soils show no signs of strength loss during shearing and have a peak undrained shear strength ratio of about 0.3 in simple shear loading. Although the peak undrained shear strength ratio for the foundation soils is lower than the peak undrained strength for the tailings, the foundation soils show no signs of strength loss and were more ductile in their response.

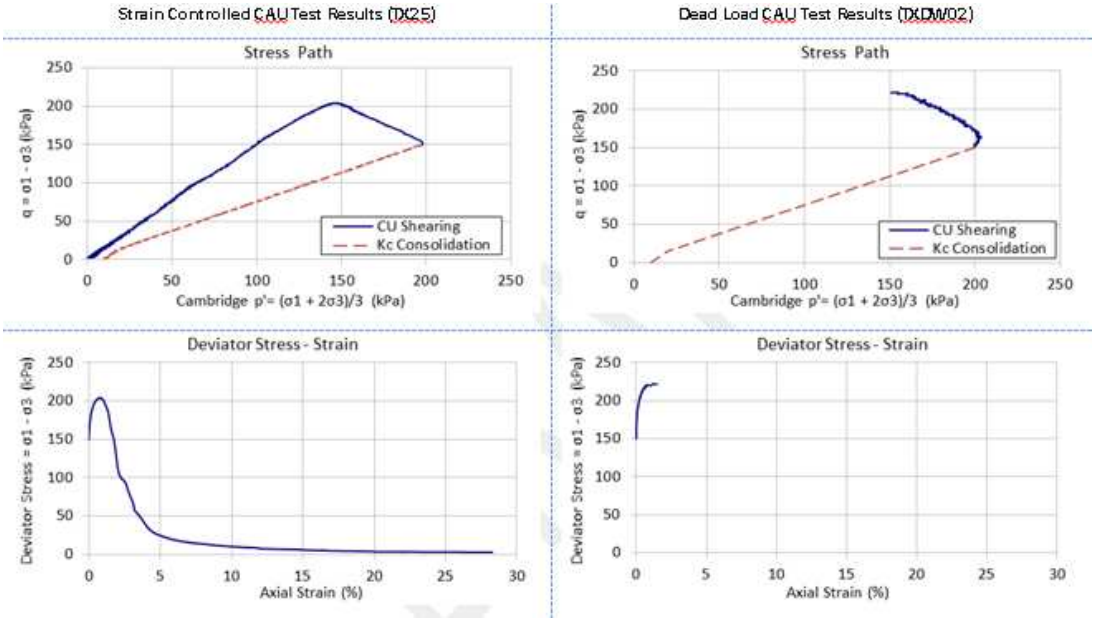

Figure 41: Comparison Between an Anisotropically Consolidated Strain-controlled (CAU-TX25) and Load-controlled Test (CAU-TXDW02) with Same State (ψ = +0.09) and Coarse Gradation

A key observation from the advanced testing is the existence of bonding in some of the samples tested. Bonding can occur due to either mechanical, chemical, or biological means. The fact that the samples were reconstituted and were less than 24 hours old before shearing suggests that bonding could be due to mechanical means because chemical and biological bonding typically take significant time to form. However, the SEM images show that bonding is more likely due to chemical bonding from iron oxide and appears to form rapidly.

6.6 Material Parameters

Parameters were calculated from the field and laboratory data for the principal purposes of performing deformation and stability analyses to simulate the conditions prior to the dam failure and to test potential failure trigger mechanisms. Details are contained in Appendix E.

The parameters required for the various analyses are:

- *Elastic moduli and peak drained shear strength.* These parameters were derived from triaxial test data. The assigned moduli values were informed by the estimated state parameter of the tailings derived from the CPTu.

- *CS deformation analyses.* The CS and dilatancy parameters were derived from the triaxial data. The *in situ* density (or state parameter) was estimated from the CPTu data, and the elastic moduli were estimated from the bender element and Vs data.

- *Stability analyses.* Peak and liquefied undrained shear strengths and their associated strains were derived from triaxial testing data and compared with CPTu data.

An important component of the above evaluation is the estimation of the *in situ* state of the tailings prior to failure. As part of this assessment, a review of the available CPTu data was completed. This included delineation of tailings material within the dam into similar tailings types (i.e., fine and coarse tailings as discussed in Section 6.1.1). A description of how delineation was developed in two- (2D) and three-dimensions (3D) is presented in Appendix F. Details on parameter selection are provided in Appendix E.

The estimation of *in situ* state followed four different approaches. Initial estimates were made using the empirical method suggested by Robertson (2010), but it was recognized that the unusual mineralogy of the tailings would likely make these estimates unreliable. A second approach was applied using the laboratory bender element (Vs) results combined with the field measured Vs values. However, this methodology was questionable due to the lack of sensitivity to variations in the *in situ* Vs measurements. A third approach was applied using the method suggested by Plewes et al. (1992), since this method allows input of the specific CSL parameters, which were available from the advanced laboratory testing. However, this too presents reliability issues since the mineralogy and other properties of the tailings are different than the historical data used to develop the relationships. The final approach applied was the full inversion of the CPTu results using CS parameters obtained from the advanced laboratory testing and applying the approach suggested by Jefferies and Been (2016). This involves using cavity expansion to obtain estimated state parameters from CPTu. This has the ability to account for the unique material behavior captured in the advanced laboratory testing. This final approach was considered to be the most reliable. A summary of the estimated state parameters for the coarse and fine gradations is shown in Figure 42, along with histograms used in the analysis. The resulting average state parameters are -0.02 for the coarse gradations and +0.16 for the fine gradations. All methods show that the fine tailings have a looser state than the coarse tailings.

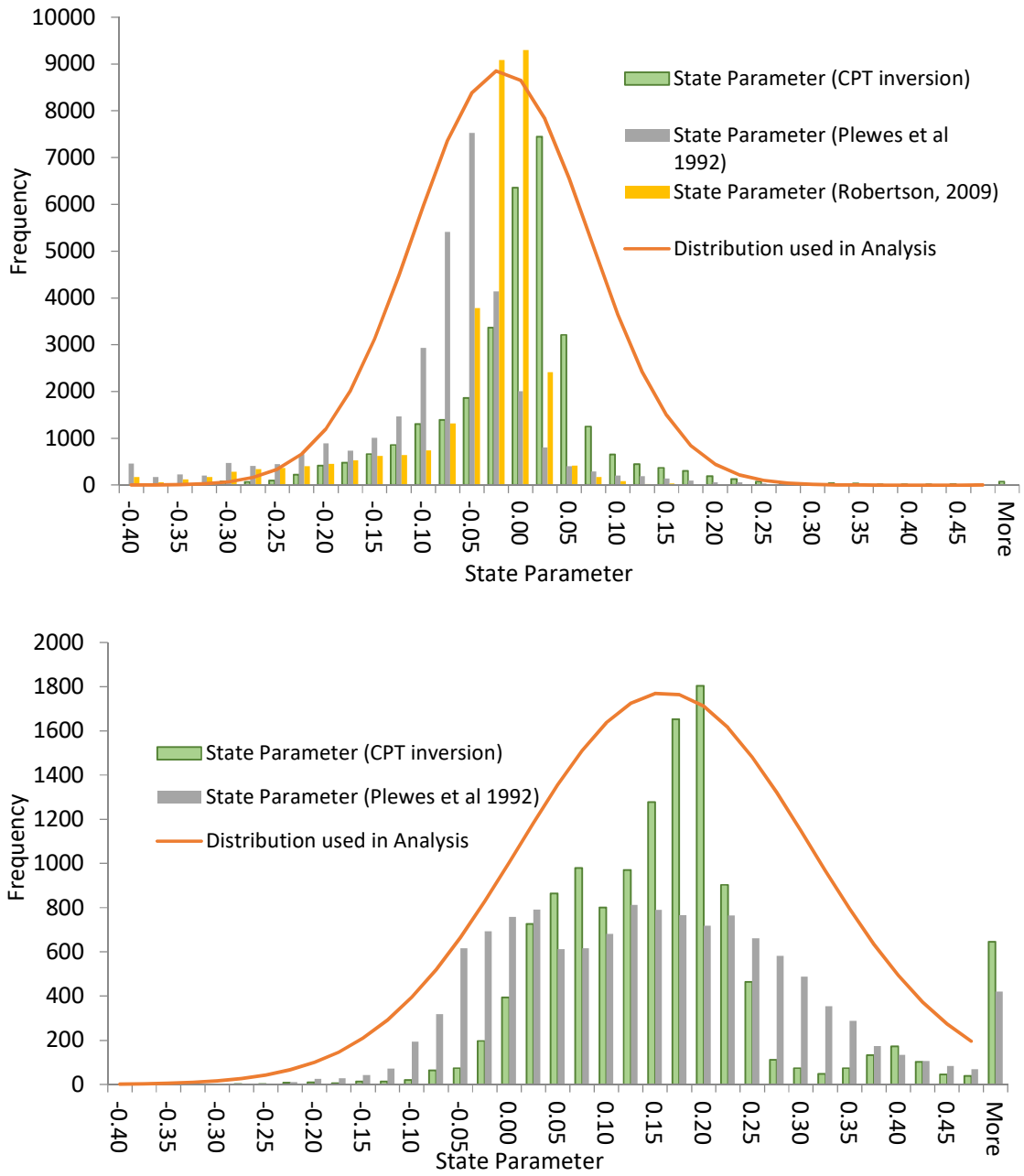

Figure 42: Cumulative Distribution of State Parameters for Coarse and Fine Gradations

Results from anisotropically consolidated undrained triaxial tests were used to develop relationships between peak and liquefied undrained strength ratio, as well as the strain required to reach both peak and liquefied strengths and the state parameter for the samples, because this was required for the subsequent deformation computer modeling, as described in Section 8.

7 WATER MOVEMENT WITHIN DAM I PRIOR TO FAILURE

7.1 Introduction

Water plays an important role in the stability and behavior of the dam. The historical data show that water levels within the dam were generally high, especially near the toe of the dam, with seepage observed from the face of the dam. Hence, detailed analyses were carried out to better understand the movement of water within the dam, considering all the measurement records from the piezometers, water level indicators, and CPTu data.[13]

A primary objective of the design and construction of any upstream tailings embankment is to keep the phreatic surface (water level) as low as possible.[14] This principle is illustrated in Figure 43.

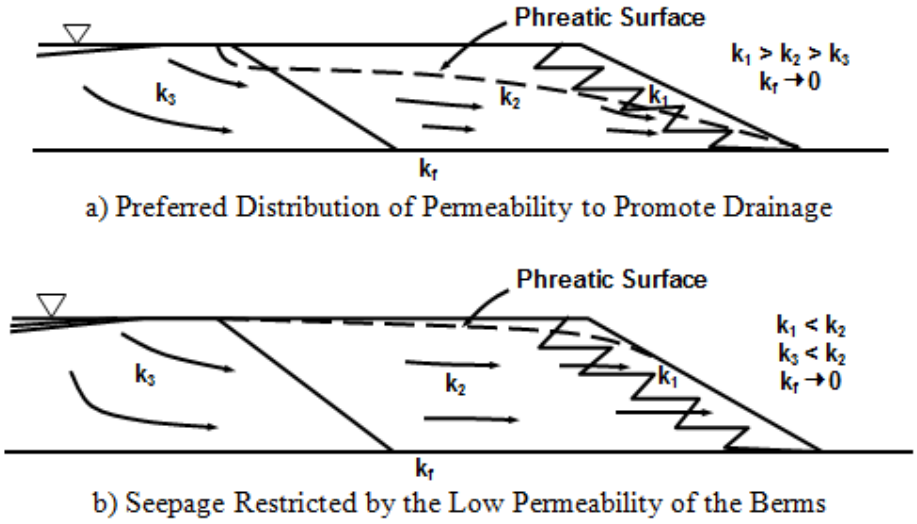

Figure 43: Influence of Internal Zoning on the Phreatic Surface (Modified from Vick, 1990)

The Panel developed comprehensive computer models to evaluate the saturated/unsaturated seepage regime in Dam I based on the available field and laboratory measurements, as described in more detail in Appendix G.

7.2 Approach

Water movement within Dam I was modeled and evaluated using computer programs for modeling rainfall infiltration and seepage. The approach consisted of preliminary modeling to establish the influence of geometry, material properties, boundary conditions, model sensitivities, and general performance, followed by 2D and 3D seepage analyses.

---

[13] Certain historical reports suggest the existence of a complex system of perched water levels within the dam prior to failure. The Panel considered such a condition to be unlikely to exist.

[14] Vick, S. (1990). *Planning, design, and analysis of tailings dams.* Richmond, BC: BiTech Publishers.

After tailings deposition ceased in mid-2016, rainfall infiltration and seepage from the dam controlled the water levels in the dam. Further details for the evaluation of the surface boundary conditions and seepage models can be found in Appendix G.

7.3 Rainfall and Infiltration

Rainfall for the three years before the failure was based on the data from the automated rainfall gauges F11 and F18. Based on these rainfall records, the average rainfall at Dam 1 was about 1400 mm per year. In 2018, the wet season was more intense than in the previous three years. Details are provided in Appendix G.

A one-dimensional (1D) soil-atmosphere simulation was carried out using climate data obtained from nearby weather stations, as detailed in Appendix C, coupled with the surface hydraulic properties derived from field and laboratory testing, as described in Appendices E and G. The results of the simulation indicate a net infiltration of approximately 50% of rainfall, which was used as a surface boundary condition for the saturated/unsaturated seepage models described in the following sections.

7.4 Two-dimensional Analyses

A critical component for the development of a comprehensive seepage model is the calibration with historic piezometric levels and CPTu dissipation results measured in the dam prior to failure. Figure 44 shows the location of the piezometers and water level indicators on the dam selected for calibration, as well as the CPTu data that had dissipation tests. The piezometers and water level indicators were selected based on the reliability of the data using criteria of known location and installation, and continuity of measurements.

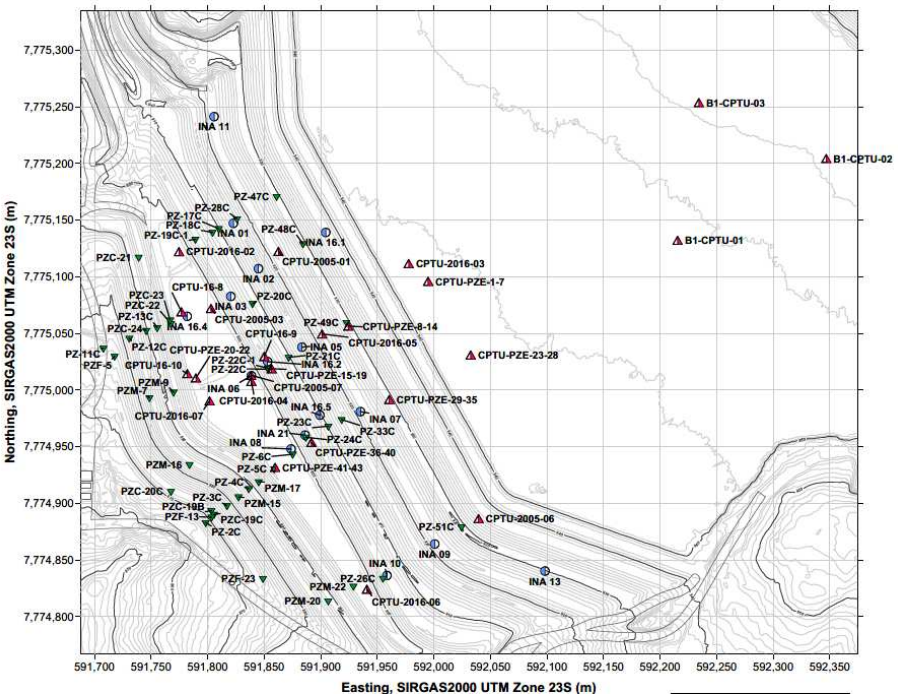

Figure 44: Location of Selected Piezometers, Water Level Indicators, and CPTus Used for Seepage Calibration

To evaluate changes in water levels in the dam, the piezometer and water level indicator readings were grouped by location. The grouping comprised all piezometers and water level indicators located on the dam either above or below Elevation 900 m msl. This essentially combines piezometers and water level indicators that were either installed above the setback or on and below the setback. The resulting mean water levels measured during the three years prior to failure are plotted on Figure 45. The data were referenced to the final reading in January 2019.

Figure 45 shows that there was a gradual decline in the mean water level since 2016. The decline was about 1.4 m for the installations above the setback (900 m msl) and about 0.5 m for the installations on or below the setback. This observation is attributed to a slow net drawdown of water after tailings deposition ceased in 2016. The water appears to be draining from the upper portions of the dam toward the lower portions. The drawdown also creates an increasing unsaturated zone in the upper portions of the dam. Figure 45 also shows minor short-term increases in water level that appear to be linked to responses during the wet seasons.

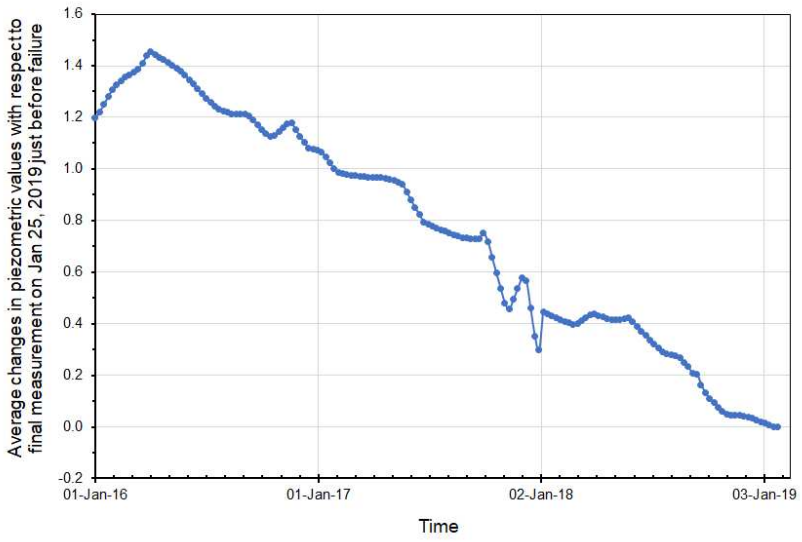

a) Changes in Piezometers and Water Level Indicators Above 900 m msl

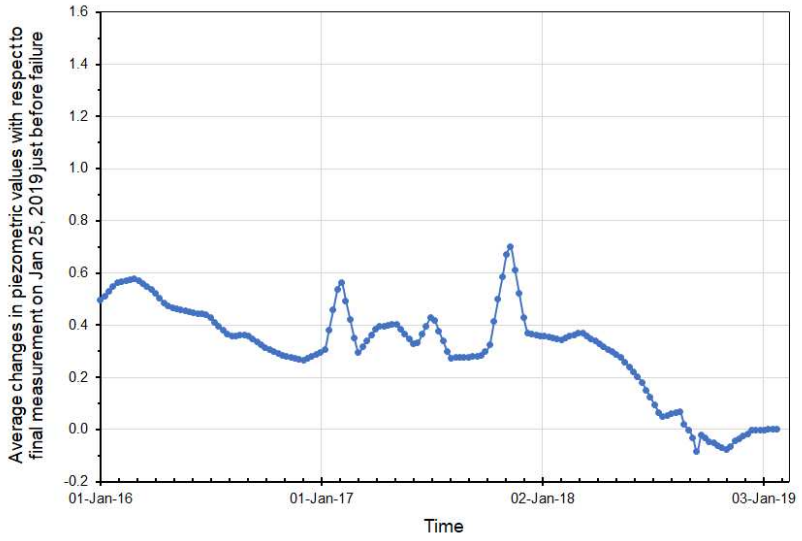

b) Changes in Piezometers and Water Level Indicators Below 900 m msl

Figure 45: Mean Piezometric and Water Levels Relative to Final Measurements on January 25, 2019

The 2D seepage models were established based on the cross-section shown in Figure 24.

An example of a recreated cross-section (3-3) is shown in Figure 24 that illustrates a complex layering of coarse and fine tailings underlying the dam extending approximately 200 m upstream. Soil parameters were based on the available field and laboratory data, and were varied to calibrate the seepage model until the calculated water pressures matched the measured

values from the piezometers and CPTu dissipation tests. Infiltration was determined to be 50% of the average annual rainfall of 1400 mm/year, based on the climate and tailings properties described previously. An example of the resulting calibration (for cross-section 3-3) is shown in Figure 46.

Based on field and laboratory data, the coarse tailings were assigned a saturated horizontal permeability (k_h) of $5x10^{-6}$ m/s while the fine tailings were assigned a k_h of $1x10^{-7}$ m/s. To reflect differences in permeability in the vertical and horizontal directions, the tailings were assigned a ratio of $k_h = 5k_v$, where k_v is the saturated permeability in the vertical direction. The interlayered structure of the tailings restricts downward drainage and promotes lateral drainage toward the downstream face of the dam. Drainage is further restricted by the relatively low permeability assigned to the compacted material in the berms, which varies from $5x10^{-7}$ m/s to $1x10^{-9}$ m/s.

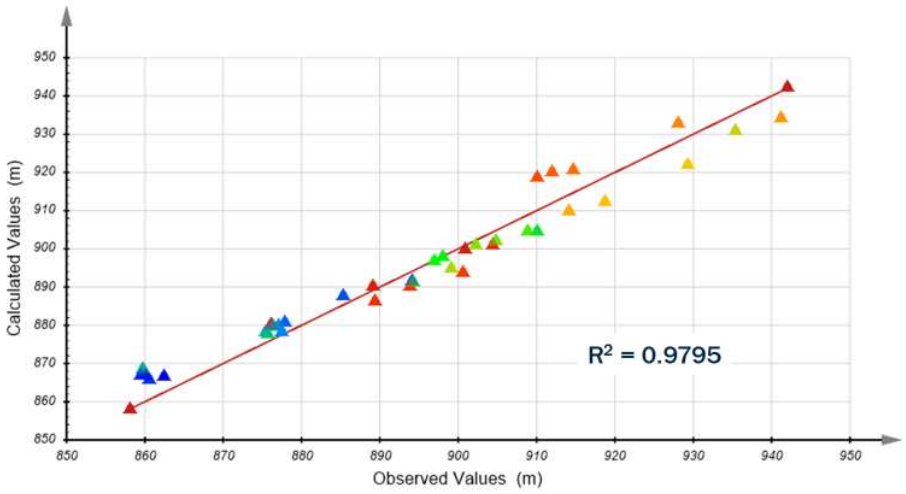

Figure 46: Calculated Versus Observed Piezometer Values for a 2D Seepage Model on Cross-section 3-3

A strong correlation was found between the measured and computed water levels that provides confidence in the accuracy of the 2D saturated/unsaturated seepage model.

Figure 47 presents a summary of the results for the 2D numerical simulation for cross-section 3-3.

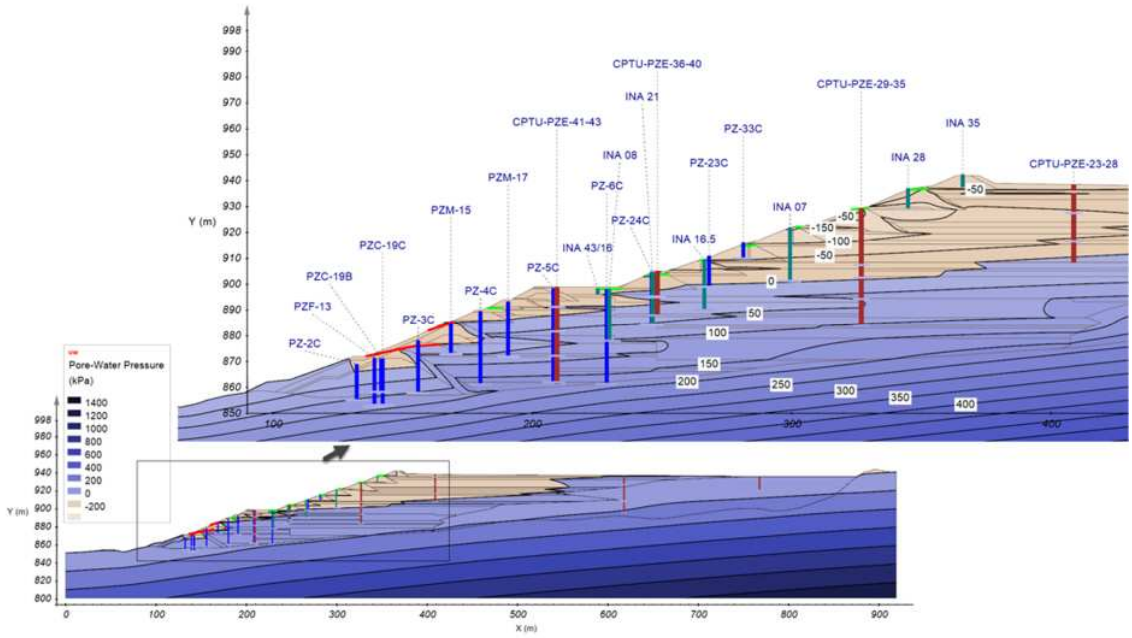

Figure 47: Computed Water Pressures from the 2D seepage model for Cross-section 3-3

The effect of poor downward drainage and restricted flow at the berms is clearly apparent in the results of the simulation presented in Figure 47. The water level shown in Figure 47, which matches the piezometer readings as well as the CPTu dissipation measurements, is high in the toe region of the dam and below the setback. The seepage analysis shows that a significant portion of the dam was saturated with a high water level, especially in the toe region.

Although the position of the water level and associated seepage on the downstream face of the dam does not change significantly, high rainfall produces a loss of (matric) suction in the unsaturated zone above the water level. The climate regime near the dam features distinct wet and dry seasonal rainfall periods that cause the suction profile in the unsaturated zone to decrease and increase. Furthermore, long-term fluctuations in the annual rainfall are superimposed on these seasonal variations, and the suction profile in the unsaturated zone is considered transient and variable.

2D computer analyses, using rainfall data from January 2016 to January 2019, were carried out to evaluate changes in soil suctions above the water level. Figure 48 shows an example profile at a location near the crest of the dam at cross-section 3-3 and shows that the computed values of suctions in the unsaturated zone decrease significantly as rainfall infiltrates the unsaturated materials. The loss in suction associated with infiltration is in the order of 50 kPa, which in turn reduces the unsaturated shear strength in this zone by about 10 kPa to 15 kPa. The impact of this loss of strength in the unsaturated zone is discussed further in Section 8. Figure 48 also illustrates that the average water pressure below the water level can be approximated by a 50% hydrostatic pressure profile.

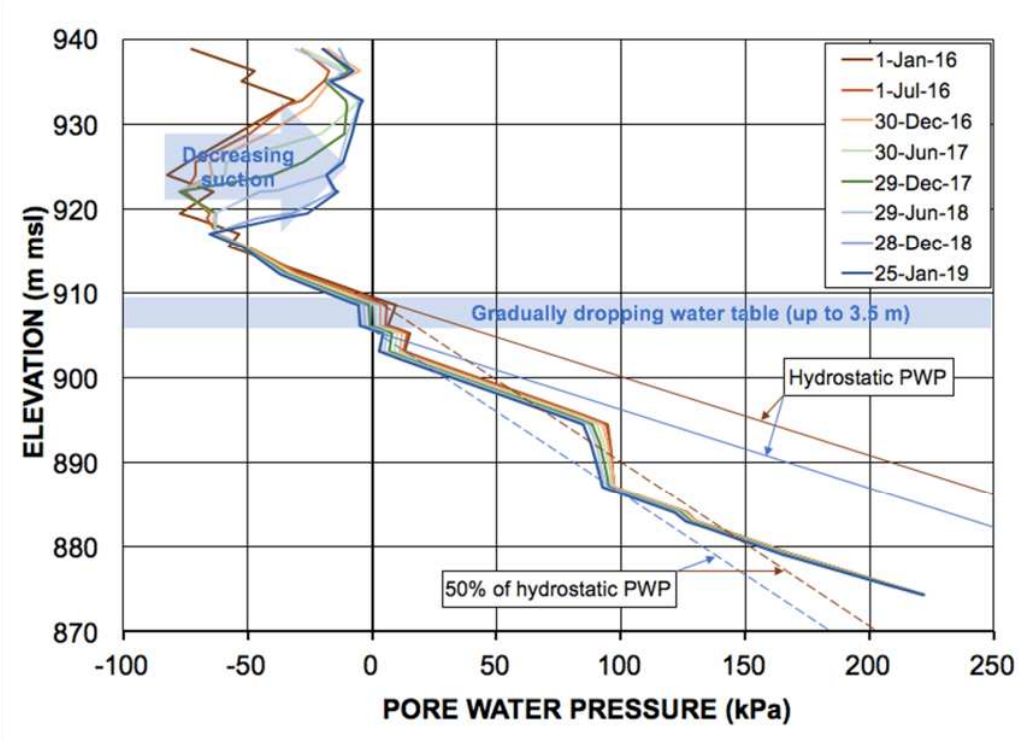

Figure 48: Pore-water Pressure Profile Beside Top Berm on Cross-section 3-3

7.5 Three-dimensional Analyses

A 3D model was also created to evaluate the flow regime in three dimensions that allows a better representation of the curved structure of the dam, the underlying natural ground topography, and the location of the drains in the model.

The material properties, infiltration rate, and layering utilized for the 3D seepage model were the same as those utilized in the 2D computer model. The results of the 3D simulations indicated a slightly lower water level in some locations compared to the 2D simulations. This was attributed to the difference in the location of the pond between the 2D and 3D models. The location and size of the pond in the 3D model represent a smaller area than the pond used in the 2D simulations. The calibration of the 3D model had similar agreement with the measured data as the 2D models.

7.6 Observations of the Analyses

The key observations of the seepage modeling for water movement in the dam are summarized as follows.

- The interbedded coarse and fine tailings layers, coupled with the low permeability of the berms, impeded drainage of the dam.

- The infiltration of 50% of the average annual rainfall was found to give a good calibration with measured water levels within Dam I and thus was considered a reasonable assumption.

- The combination of high rainfall and infiltration, and the absence of drainage produced high water levels, especially in the toe region of the dam.

- A zone of unsaturated tailings was found to be present near the crest of the dam.

- Although the position of the water level and associated seepage on the downstream face of the dam does not change significantly over time, high rainfall and infiltration decrease the suctions in the unsaturated zone. The loss in suction associated with rainfall infiltration is in the order of 50 kPa, which in turn reduces the shear strength in this zone by 10 kPa to 15 kPa.

The results of the seepage analyses were used to inform and guide the detailed deformation analyses described in Section 8.

8 STABILITY AND DEFORMATION ANALYSES – INVESTIGATING VARIOUS TRIGGERS

8.1 Approach

The Panel investigated potential triggers by creating 2D and 3D computer models of the dam. Based on historical data, detailed cross-sections were recreated to capture the distribution of materials within the dam, as described in Section 6.2. The 2D and 3D deformation models were created from these cross-sections. The purpose of these models was to evaluate possible liquefaction triggering mechanisms. The stability and deformation analyses are discussed in detail in Appendix H.

8.2 Stability of Dam I

The traditional approach to evaluate the stability of a dam is to apply Limit Equilibrium Methods (LEM). LEM assumes that the materials have a well-defined value for shear strength, and the method does not account for any deformations to generate that strength (i.e., LEM assumes that the materials are rigid and perfectly plastic). For materials that have a stress-strain relationship that increases to a single value of strength with no strength loss, this assumption is reasonable. It is common practice to use commercial software to perform LEM, and these programs allow input of a range of soil layers and groundwater conditions and will search for the failure surface that has the lowest FS. The calculated FS in those models is the average value along the failure surface evaluated. Depending on geometry, groundwater conditions, and layering, areas on the failure surface can have either higher or lower local FS values. These programs can be performed in 2D and 3D.

Historical stability calculations using LEM performed prior to the failure that used an undrained strength ratio of $s_u/\sigma'_{vo} = 0.26$ calculated an FS close to 1.0.[15] However, if the FS was very close to 1.0, the dam would be expected to show various signs of distress, such as cracking and deformations, because the materials must strain (deform) to reach their peak strength. The fact that the dam showed no signs of distress prior to failure suggests that the results of traditional LEM were misleading.

The laboratory data presented in Section 6.4 show that the materials within the dam exhibited bonding and were susceptible to significant strength loss. Hence, the materials have a high peak strength at small strains but very low shear strength at large strains (liquefied strength). The amount of strain (deformation) required to exceed the peak strength is very small. In conditions where a significant portion of the materials in the dam have a potential for significant strength loss, the results of LEM can be misleading.

In these cases, there can be regions along the failure surface that have exceeded the peak strength and have a local FS less than 1.0. If the LEM is performed using the peak strength, a high FS can be calculated that does not reflect the likelihood of instability. Re-analysis of the stability of Dam I using the peak undrained strength values determined from laboratory testing performed by the Panel, which reflect the additional strength due to bonding, resulted in a FS close to 1.5. However, this ignores possible regions of high shear stress where the local FS can be less than 1.0. The additional strength due to bonding essentially allows a steeper slope to be constructed without signs of distress, even though it could be potentially unstable. Instability can result when an event triggers undrained strength loss in parts of the slope. The larger the strength loss and the higher the stresses in the dam, the more sudden and rapid the potential failure.

Figure 49 schematically shows the different approximate stress-strain and stress-path responses for soils that have no strength loss, strength loss with no bonding, and significant strength loss due to bonding. Materials that have no strength loss will typically show significant deformation prior to failure. Materials that have strength loss with no bonding show less deformation before failure compared to the materials with no strength loss. Materials that have significant strength loss due to bonding tend to show very little deformation before failure and require very little strain to trigger the strength loss.

[15] See, e.g., 2018 TÜV SÜD Periodic Safety Review.

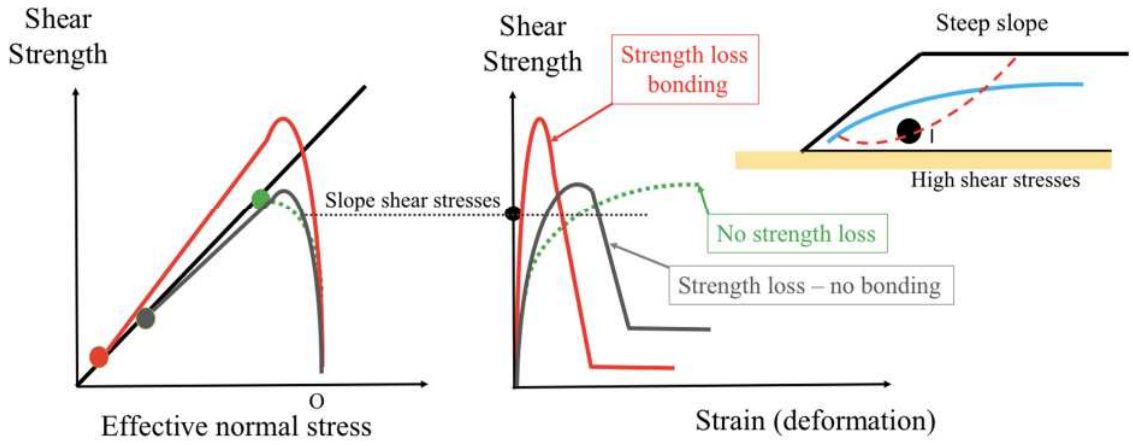

Figure 49: Schematic Comparison in Behavior Between Soil that has No Strength Loss, Soil with Strength Loss, and Either No Bonding or with Bonding

8.3 Deformation Analysis of Dam I

8.3.1 Overall Approach

To avoid the limitations of the LEM approach, deformation analyses can be performed to capture possible strength loss in the materials. This requires more complex numerical modeling that includes representative stress-strain relationships for each material type in the dam. These analyses can be performed in 2D and 3D; the Panel focused on 3D modeling.

8.3.2 Evaluation of Triggering Mechanisms

8.3.2.1 Initial Evaluation

Before starting the analyses, the triggering mechanisms described in Section 3.3 were reviewed to eliminate mechanisms that were not viable. The following mechanisms could be evaluated without the need for detailed computer analyses.

Rapid loading, such as dam construction or tailings deposition

No dam construction occurred after 2013, and tailings deposition ceased in July 2016. Hence, rapid loading was not a viable trigger.

Rapid cyclic loading, such as earthquakes or blasting

Evaluation of the seismograph records from the day of the failure showed that no earthquakes and no blasting were recorded prior to the first observation of the failure. Details are provided in Appendix I. Hence, earthquakes and blasting were not considered viable triggers. There is small seismic activity registered less than 30 s prior to the first observed deformations, which is considered to be the result of internal strength loss occurring in the dam prior to the visible manifestation of the failure.

Fatigue loading, such as repeated blasting

Although on the day of the failure no blasting was recorded before the first observed deformation, it is known that regular blasting occurred at several pits in the area. There is the potential that repeated blasting could induce cumulative strains in the dam. However, analysis of the nearby seismograph records from previous blasts, as detailed in Appendix I, show that the strains induced in the tailings would not have exceeded the threshold strain level of the tailings and the behavior of these materials would have remained elastic and not accumulate strain. Hence, fatigue loading from repeated blasting in the area is not considered a viable trigger.

Unloading, such as: (i) rising water levels within the dam; (ii) deformations within the foundation; or (iii) the presence of weak layers

Piezometer and water level indicators show that the water levels were slowly dropping in the three-year period prior to failure. Details are provided in Appendix G. The testing carried out by the Panel showed no indication of continuous weak layers in the natural soils beneath the dam, and the laboratory testing showed no indication of strength loss in these soils. As described in Section 5, the analysis of InSAR data shows that the deformations in the one-year period prior to failure were small, slow, and predominantly in the vertical direction. The horizontal deformations near the toe of the dam were mostly less than 10 mm/year over that period, but included some small areas with up to 30 mm/year. This indicates that there were no significant horizontal deformations that might have been linked to deformations in the foundation or due to weaker layers. Although the materials in the dam are composed of interlayered coarse and fine tailings, the laboratory testing and *in situ* shear wave velocity data show that the fine tailings have similar stiffness and compressibility to the coarse tailings. Hence, this layering would not induce significant differential deformations and unloading between the layers. Accordingly, unloading mechanisms were not viable triggers.

Internal erosion and piping

There was no evidence of internal erosion or piping associated with the failure. Although seepage from the face of the dam did occur, the rate of seepage was generally slow and measured volumes from flow drains installed at the dam did not increase with time, and neither increasing nor significant discharge of fines were observed near the time of failure. The observed failure mechanism from the video images was inconsistent with internal erosion and piping. Hence, internal erosion and piping were not viable triggers.

8.3.2.2 Detailed Evaluation Using Computer Modeling

The following mechanisms were taken forward for detailed assessment in the deformation modeling:

- Human interaction, such as drilling of vertical boreholes and installation of DHPs;
- Localized loss of strength due to inflow of water from underground springs;

- Loss of suction and strength in the unsaturated zone above the water table; and
- Internal creep due to cumulative strains that develop under a constant load.

The objective of the deformation analyses was to evaluate the most likely trigger of instability, consistent with all of the available data and observations. Since the dam showed no signs of distress prior to failure, yet failed suddenly, it was recognized that the trigger event could be relatively small. The computer model was created to match the pre-failure conditions at the dam, taking into consideration all the available data on layering, soil variability, water pressures, and material parameters, as well as known pre-failure events at Dam I that did not trigger instability. This allowed the Panel to evaluate and identify the most likely trigger.

The approach included the following three stages:

Stage 1 – Establish pre-failure conditions

- Develop the model geometry to match the tailings layering described previously;
- Develop material parameters for these layers that match the behavior of brittle strength loss observed from laboratory testing and use these to assign model parameters;
- Apply the drained strength parameters;
- Assign spatial and statistical variations of the key material parameters in accordance with variations calculated from the CPTu data; and
- Determine the pre-failure stress states throughout the dam by constructing the dam in the model in a manner that is consistent with the construction history.

Stage 2 – Initial screening of various liquefaction triggering mechanisms

- Establish an extreme condition by assigning undrained strength parameters below the water level;
- Based on laboratory test results, assign a distribution of peak undrained and liquefied strengths to the tailings layers, as well as define the distribution of strains required to cause a loss of strength to occur;
- Calibrate the model based on pre-failure activities; and
- Assess, using computer simulations, the potential for each of the possible triggering mechanisms to cause a loss of undrained strength in a manner consistent with the events prior to failure and to match the observations during failure.

Stage 2 of the analysis was based on a simplifying assumption that the undrained strengths were mobilized throughout the entire dam and that the dam had a small margin of stability before the possible triggering mechanism occurred. The purpose of this stage was to test the

effect of the possible triggers on the dam in this condition. This approach enabled the Panel to assess which of the possible triggers would not have had a meaningful impact on the stability of the dam even under this somewhat extreme condition, thereby reducing the number of potential triggers for further evaluation.

Stage 3 – Detailed assessment of most likely triggering mechanism(s)

- Assess, using computer simulations, the remaining possible triggers that had a significant impact on the stability of the dam in the simplified Stage 2 analyses; and
- Include creep deformations under high shear stresses observed from the advanced laboratory testing.

8.3.3 Stage 2 Deformation Analyses

The deformation analyses included statistical and spatial distributions of strength that are consistent with the distributions seen in the CPTu data. Multiple simulations were required to obtain representative models that matched the pre-failure observations and used the undrained response determined from the advanced laboratory testing.

Pre-failure Activities

To assist in calibrating the model, the Panel identified two activities in the months prior to the failure that are known not to have triggered the failure:

- DHP 15 installed in June 2018; and
- The drilling of borehole SM-09 in early 2019.

In the analyses, as detailed in Appendix H, the installation of the DHPs was simulated by an applied water pressures of 600 kPa and 1000 kPa at the end of DHP 15. The drilling of borehole SM-09 was simulated by assuming a condition that would result in the loss of undrained strength in a 1 m radius around SM-09. Because the evidence shows that the dam was very close to failure, a computer model was considered representative of the pre-failure condition when neither of these activities caused failure, but a minor reduction in shear strength throughout the dam would have.

The resulting representative computer models were then used for testing the remaining trigger mechanisms.

Human Interaction

In June 2018, during the installation of DHP 15, a localized strength loss occurred in Dam I, as described in Section 4.4.2. Given the nature of the tailings material present within the dam, and thus around DHP 15, it is likely the material regained its strength in a short period after the incident. Reports indicate that seepage was controlled within several days, and no indication of any ongoing impact of DHP 15 is seen in drone footage recorded just one week prior to the

incident. Nonetheless, the analyses considered an extreme scenario in which strength loss occurred around DHP 15 later in January 2019, potentially triggering failure. This was assessed by assigning a condition of undrained strength loss in a 1 m radius around DHP 15. This is an unlikely scenario, and it did not lead to failure of the dam in the representative models. Hence, the Panel concluded that liquefaction surrounding DHP 15 is not a viable trigger.

The borehole being drilled at the time of the failure was SM-13. The potential for this to trigger liquefaction was assessed by enforcing a condition of undrained strength loss in a 1 m radius of the borehole down to a depth of 80 m. This condition is considered to represent an extreme scenario. This condition did not cause significant deformations or failure of the dam in the representative models. Hence, the drilling of SM-13 is not considered a viable trigger.

Underground Springs

The Panel considered a scenario in which an influx of groundwater enters the dam at the location of known, pre-existing, underground springs along the northern edge of the impoundment, which in turn causes a potential zone of strength loss in those regions. This was treated as a localized event around the springs because the piezometers did not detect a significant change in water pressure beneath the dam prior to failure.

This was simulated in the representative models by assigning a condition of undrained strength loss to the tailings within a 50 m radius around the springs. This scenario caused significant local deformations around the springs; however, it did not result in failure of the dam. The pattern of displacements resulting from this simulation did not reflect the observations of the failure obtained from the video evidence and, hence, influx of water from the underground springs was not considered a viable trigger.

Loss of Suction in the Unsaturated Zone

The seepage analysis described in Section 7 identified that a loss of suction resulting from cumulative rainfall over the years following the cessation of tailings deposition, culminating in the intense rainfall recorded towards the end of 2018, would lead to a small strength reduction in the previously unsaturated zone (i.e., the zone above the water level). This was assessed in the analysis by applying a strength reduction to the zone above the water table. Three values of strength reduction were assessed: 5 kPa, 10 kPa, and 15 kPa. The strength reduction was assessed as being no greater than 15 kPa. It was found that a reduction in strength of 5 kPa caused only minor deformations of the dam; however, a strength reduction of up to 15 kPa in this zone caused larger deformations in the region where the failure occurred. This analysis showed that a significant loss of suction could potentially have contributed to the observed failure mechanism and required further analysis in Stage 3.

Stage 2 of the analysis showed that events that caused localized loss of strength in the marginally stable condition of the dam generally did not lead to overall instability. The more widespread, possible trigger of loss of suction was analyzed further in Stage 3. Because creep

as a possible failure mechanism is more global in nature, it was not tested in Stage 2 but was evaluated in detail in Stage 3.

8.3.4 Stage 3 of Deformation Analyses

Stage 3 involved assessing a condition that was observed in the laboratory in which loose samples of tailings continued to accumulate strain under a constant, high shear stress. This accumulation of strain under constant load is referred to as creep. The rate of creep depends on the state (density) of the material and the level of shear stress. Materials that are loose can accumulate significant creep strains under high shear stresses. For a material that can have a significant strength loss, the accumulation of internal strains under constant load can ultimately lead to creep rupture. Creep rates based on the advanced laboratory tests were incorporated into the computer simulations using the reference models identified in Stage 2.

The influence of creep was evaluated in three cases: i) independently; ii) in association with a strength reduction in the unsaturated materials above the water level due to rainfall infiltration; and iii) in combination with the drilling of borehole SM-13. Computer simulations showed that creep on its own was capable of triggering the failure but the resulting deformations do not match well the observed deformations. The addition of the drilling of borehole SM-13 had no significant impact on stability of the dam in the simulations. Computer simulations combining accumulated strains due to creep with strength reduction in the unsaturated materials above the water level due to rainfall infiltration showed that while creep was the more dominant contributing factor leading to the failure of the marginally stable dam, strength reduction in the unsaturated materials made an important contribution.

Figure 50 shows the calculated pre-failure deformations due to creep combined with a 15 kPa strength reduction due to loss of suction on cross-section 3-3, based on the 3D computer simulations. The calculated pre-failure deformations are small in magnitude and show a similar trend as those evaluated from the InSAR analyses (shown in Figure 20). The computer simulations show that deformations due to creep prior to failure can be small. Figure 51 shows the calculated deformations at failure due to creep combined with a 15 kPa strength reduction due to loss of suction in cross-section 3-3, based on the 3D computer simulations. Figure 51 shows a calculated failure mechanism that closely matches the observed deformations at failure from the video evidence, confirming that a combination of creep and strength reduction due to intense rainfall towards the end of 2018 best explains the failure of the marginally stable dam.

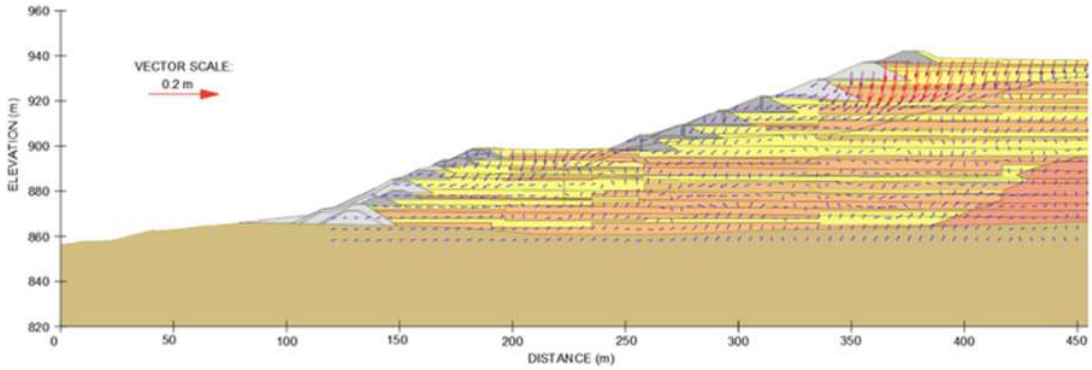

Figure 50: Cross-section 3-3 Showing Calculated Pre-failure Deformations Due to Creep Combined With a 15 kPa Strength Reduction From Loss of Suction from 3D Computer Simulations

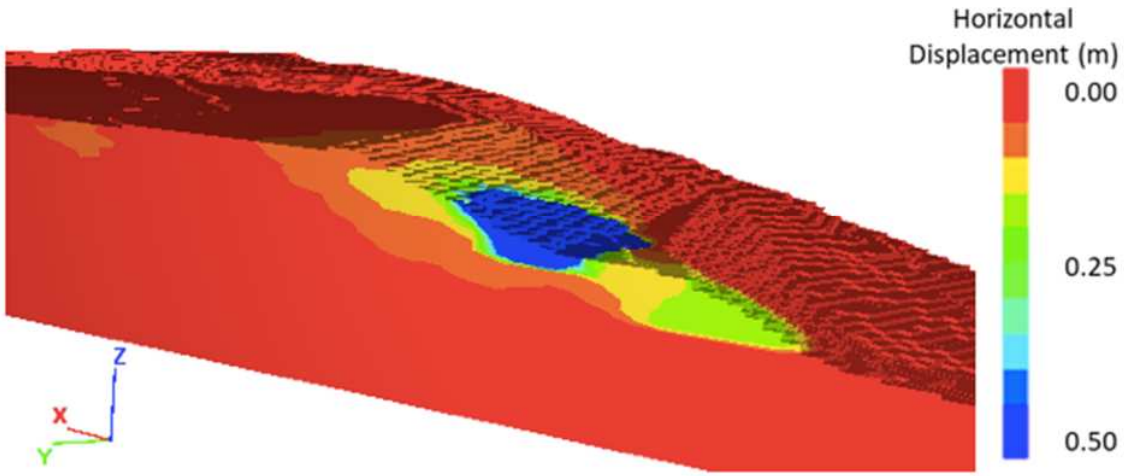

Figure 51: Cross-section 3-3 Showing Calculated Deformations at Failure Due to Creep Combined With a 15 kPa Strength Reduction From Loss of Suction from 3D Computer Simulations

The evidence shows that the failure on January 25, 2019 was due to a combination of ongoing creep and a small strength reduction in the unsaturated zone caused by the cumulative rainfall since the end of tailings deposition, including the intense rainfall towards the end of 2018.

The Panel also conducted an analysis to evaluate the deformation after the failure using the Material Point Method (MPM). This analysis used a similar strain weakening relationship as used in the deformation analyses. The MPM replicated the progression of the failure in approximately the first 5 s of deformation.

9 CONCLUSIONS

Experience from previous tailings dam failures shows that they are rarely due to one cause. The following history created the conditions for instability in Dam I:

- A design that resulted in a steep upstream constructed slope;
- Water management within the tailings impoundment that at times allowed water to get close to the dam crest, resulting in the deposition of weak tailings near the crest;
- A setback in the design that pushed the upper portions of the slope over weaker fine tailings;
- A lack of significant internal drainage that resulted in a high water level in the dam, particularly in the toe region;
- High iron content, resulting in heavy tailings with bonding between particles. This bonding created stiff tailings that were potentially very brittle if triggered to become undrained; and
- High and intense regional wet season rainfall that can result in a loss of suction, producing a small loss of strength in the unsaturated materials above the water level.

The Panel addressed the following three questions:

- Why did a flow slide occur?
- What triggered the failure?
- Why did the flow slide occur when it occurred?

The Panel found that the failure and resulting flow slide was the result of flow liquefaction within the tailings in the dam. The history described above created a dam that was composed of mostly loose, saturated, heavy, and brittle tailings that had high shear stresses within the downstream slope, resulting in a marginally stable dam (i.e., close to failure in undrained conditions). Laboratory testing showed that the amount of strain required to trigger strength loss could be very small, especially in the weaker tailings. These were the main components that made it possible for flow liquefaction. The remaining component was either an event, or combination of events, that would trigger undrained strength loss in the tailings.

The Panel concluded that the sudden strength loss and resulting failure of the marginally stable dam was due to a critical combination of ongoing internal strains due to creep, and a strength reduction due to loss of suction in the unsaturated zone caused by the cumulative rainfall since the end of tailings deposition, including the intense rainfall towards the end of 2018. This followed a number of years of increasing rainfall after tailings deposition ceased in July 2016. The internal strains and strength reduction in the unsaturated zone reached a critical level that

resulted in the observed failure on January 25, 2019. The calculated pre-failure strains and deformations from internal creep match the observed small deformations on the dam in the year prior to the failure.

10 QUESTIONS

The Panel was specifically asked to respond to a series of questions.

1. What role (if any) did the construction, raising, and/or design of Dam I play in the technical cause(s) of the failure of Dam I?

The design and construction of Dam I is a contributing factor to its failure. Specifically, the design resulted in a dam that was steep with a lack of sufficient drainage, resulting in high water levels, both of which caused high shear stresses within the dam.

2. What role (if any) did drainage and/or lack of drainage play in the technical cause(s) of the failure of Dam I?

Dam I did not contain sufficient internal drainage and therefore had a high water level in the downstream slope. This resulted in a significant portion of the tailings remaining saturated, which is a prerequisite for undrained flow liquefaction.

3. What, if anything, do the data from various monitoring devices at Dam I (including piezometers) during the 12 months prior to the failure indicate about the technical cause(s) of the failure of Dam I?

None of the monitoring devices detected precursors to failure. Rather, the dam's failure was sudden and abrupt, which was the result of high shear stresses in the downstream slope of the dam and the brittle, undrained response of the tailings.

4. Did deformations or movement occur at the Dam I site within the 12 months prior to the failure? If yes, what did these deformations or movements indicate about the technical cause(s) of the failure of Dam I?

Dam I showed no signs of distress, such as large deformations resulting in cracking and bulging, prior to failure. The analysis of the InSAR data showed that there were small deformations occurring in the 12-month period prior to failure and that these deformations were primarily in the vertical direction. These deformations were too small and too slow to be detected by the ground-based radar and the other monitoring devices typically used at tailings dams. The small deformations allowed the Panel to rule out movements in the natural soils beneath the dam and weaker layers within the dam as triggers for the failure. These small deformations were not a precursor to failure, but were consistent with ongoing internal creep.

5. What role (if any) did activities occurring at, near, or around Dam I in the 12 months prior to the failure play in the technical cause(s) of the failure? If activities at the Dam I site did play a role, which activities?

a. What role (if any) did the installation of deep horizontal drains (DHPs) play in the technical cause(s) of the failure of Dam I?

The Panel's analyses of DHP 15 showed that the installation of DHPs were not likely to have played a role in the failure of the dam.

b. What role (if any) did the incident that occurred on June 11, 2018, during the installation of DHP 15 play in the technical cause(s) of the failure of Dam I?

The Panel's analysis revealed that the incident that occurred during the installation of DHP 15 did not play a role in the failure of the dam. The strength loss that occurred as a result of the incident was localized and there was no indication of any ongoing impact of DHP 15 after remediation was undertaken in the days following the incident.

c. What role (if any) did drilling occurring on January 25, 2019, on Dam I play in the technical cause(s) of the failure of Dam I?

The Panel's analysis of the vertical borehole drilled on the day of the failure showed that the drilling activity was not sufficient to trigger the observed failure of the dam. The effect of the drilling was localized and did not result in global instability.

6. Did seismic events play a role in the technical cause(s) of the failure of Dam I? If yes, was the seismic activity attributable to detonations occurring near Dam I?

No. A review of the seismograph data from the day of the failure indicated that no earthquake or blasting activity were recorded prior to the failure.

ACKNOWLEDGEMENTS

The Panel would like to express our appreciation to the consultants (Geosyntec Consultants; Klohn Crippen Berger Ltd. (KCB); Bentley Systems (formerly known as SoilVision); and Geoapp s.r.l.) who provided engineering, modeling, and organizational assistance. We would especially like to recognize the contribution of Dr. Joe Quinn of KCB for his outstanding analytical modeling as well as his role in the field and laboratory studies.

The Panel would also like to acknowledge the sacrifices of the victims, their loved ones and those affected by this tragedy. We can only hope that our work may contribute to understanding the technical causes of this failure and help prevent similar occurrences from happening again.